Elevated $FOXG_1$ and SOX_2 in glioblastoma enforces neural stem cell identity through transcriptional control of cell cycle and epigenetic regulators

Title: Elevated FOXG1 and SOX2 in glioblastoma enforces neural stem cell identity through transcriptional control of cell cycle and epigenetic regulators

Harry Bulstrode[1], Ewan Johnstone[2], Maria Angeles Marques-Torrejon[1], Kirsty M. Ferguson[1], Raul Bardini Bressan[1], Carla Blin[1], Vivien Grant[1], Sabine Gogolok[1], Ester Gangoso[1], Sladjana Gagrica[3], Christine Ender[3], Vassiliki Fotaki[4], Duncan Sproul[5], Paul Bertone[2], Steven M. Pollard[1,*]

Authors Affiliations

[1]MRC Centre for Regenerative Medicine and Edinburgh Cancer Research UK Cancer Centre, University of Edinburgh, 5 Little France Drive, Edinburgh EH16 4UU, UK.

[2]Wellcome Trust – Medical Research Council Stem Cell Institute, University of Cambridge, Tennis Court Road, Cambridge CB2 1QR, UK.

[3]Department of Cancer Biology, UCL Cancer Institute, University College London, Paul O'Gorman Building, 72 Huntley Street, London, WC1E 6BT, UK.

[4]Centre for Integrative Physiology, Hugh Robson Building, George Square, University of Edinburgh, Edinburgh, UK.

[5]Medical Research Council Human Genetics Unit and Edinburgh Cancer Research Centre, Medical Research Council Institute of Genetics and Molecular Medicine, University of Edinburgh, Edinburgh EH4 2XU, UK

* Corresponding and lead author:

Steven Pollard: steven.pollard@ed.ac.uk Tel: +44 (0)131 6519544

Running title: FOXG1/SOX2 controls cell cycle and epigenetic regulators in GBM

Summary

Glioblastoma (GBM) is an aggressive brain tumor driven by cells with hallmarks of neural stem (NS) cells. GBM stem cells frequently express high levels of the transcription factors FOXG1 and SOX2. Here we show that increased expression of these factors restricts astrocyte differentiation and can trigger de-differentiation to a proliferative NS cell state. Transcriptional targets include cell cycle and epigenetic regulators (e.g. *Foxo3*, *Plk1, Mycn;* and *Dnmt1, Dnmt3b, Tet3*). *Foxo3* is a critical repressed downstream effector that is controlled via a conserved FOXG1/SOX2-bound cis-regulatory element. *Foxo3* loss, combined with exposure to the DNA methylation inhibitor 5-Azacytidine, enforces astrocyte de-differentiation. DNA methylation profiling in differentiating astrocytes identifies changes at multiple polycomb targets, including the promoter of *Foxo3*. In patient-derived GBM stem cells CRISPR/Cas9 deletion of *FOXG1* does not impact proliferation *in vitro*; however, upon transplantation *in vivo FOXG1* null cells display increased astrocyte differentiation and upregulate FOXO3. By contrast, SOX2 ablation attenuates proliferation and mutant cells cannot be expanded *in vitro*. Thus, FOXG1 and SOX2 operate in complementary but distinct roles to fuel unconstrained self-renewal in GBM stem cells via transcriptional control of core cell cycle and epigenetic regulators.

Keywords: Glioblastoma, FOXG1, SOX2, FOXO3, cell cycle, epigenetics, de-differentiation, neural stem cell, astrocyte.

Introduction

Glioblastoma multiforme (GBM) is a highly aggressive brain tumor driven by neural stem cell-like cells. It is increasingly clear that the transcriptional and epigenetic mechanisms that control the initiation and maintenance of neural stem and progenitor cells are hijacked and deregulated in GBMs (Patel et al., 2014; Singh et al., 2003; Suvà et al., 2014). Neurodevelopmental transcription factors (e.g. bHLH, SOX, FOX and HOX families) are known to be critical regulators of neural stem cell self-renewal and differentiation. Transcription factors are, however, difficult to 'drug' with small molecules. Improved understanding of the role of these master regulators and their key downstream effectors is needed.

We previously reported that *FOXG1* is one of the most consistently overexpressed genes when comparing primary cultures of GBM-derived neural stem (GNS) cells and genetically normal NS cells (Engström et al., 2012). FoxG1 is a member of the forkhead box family of transcription factors. During development, it has an essential role in regulating forebrain radial glia/ neural progenitor cell proliferation and limiting premature differentiation (Martynoga et al., 2005; Mencarelli et al., 2010; Xuan et al., 1995).

Although *FOXG1* is not genetically amplified in glioma, *FOXG1* mRNA levels in primary tumors are inversely correlated with patient survival (Verginelli et al., 2013). Recently, Liu et al. demonstrated that the oncogenic EGFR truncation (EGFRvIII) – found in a significant proportion of 'classical' subtype GBMs – operates in part by triggering expression of *FOXG1* (Liu et al., 2015). FOXG1 protein has previously been shown to operate by attenuating the cytostatic effects of TGF-beta signalling by binding and sequestration of FOXO/SMAD complexes in established glioblastoma cell lines (Seoane et al., 2004). These findings suggest that increased levels of FOXG1 in

GBM might be functionally important in driving tumor growth. Evidence in favor of this hypothesis has been provided by shRNA knockdown of FOXG1 in GBM stem cells, which leads to reduced proliferation of the resulting tumors (Verginelli et al., 2013). Despite these observations, we have poor understanding of the functional consequences of its increased levels and the downstream transcriptional targets in both NS cells and GBM stem cells.

SOX2 is an established stem cell 'master' regulator highly expressed in multiple tissue stem cells, including various types of neural stem and progenitor cells (Arnold et al., 2011). It has important functions within the pluripotent epiblast, embryonic stem cell cultures, neuroepithelial progenitors and in multipotent radial glia (fetal, postnatal and adult) (Avilion et al., 2003). In *Xenopus*, chick, and mouse, the constitutive expression of *Sox2* re-specifies gastrulation stage progenitor cells into neuroectoderm, at the expense of other lineages (Kishi et al., 2000; Zhao et al., 2004). It is genetically amplified in ~4% of GBM samples (Brennan et al., 2013). Knockdown experiments have indicated that SOX2 is required to sustain the aggressive growth and infiltrative behavior of GBMs (Gangemi et al., 2009; Alonso et al., 2011).

Together these studies point to an important role for FOXG1 and SOX2 in NS cells and their potential deregulation in GBM. FoxG1 and Sox2 are also established reprogramming factors: forced co-expression can trigger direct reprogramming of fibroblasts to an NS cell-like state (Lujan et al., 2012). The excessive levels or activity of these factors in GBM may therefore operate intrinsically to restrict tumour cell differentiation through perpetual reprogramming to a radial-glia like NS cell state. Despite the frequent expression of FOXG1/SOX2 in GBM, we have only a poor understanding of their downstream transcriptional targets and how they operate to drive proliferation and limit terminal differentiation.

Here we define genome-wide transcriptional targets of both factors, and find that FOXG1/SOX2 can act at shared target loci encoding core cell cycle and epigenetic regulators. Loss of function studies suggest they have context-specific functions, with SOX2 essential for proliferation, while FOXG1 protects cells from differentiation cues, both *in vitro* and *in vivo*. These two transcriptional regulators therefore cooperate in functionally distinct but complementary roles to limit astrocyte differentiation commitment in GBM and enforce the proliferative NS cell-like phenotype.

Results

Human GBM stem cells express elevated levels of FOXG1 and exhibit an open chromatin profile enriched for FOX/SOX motifs

To explore the role of FOXG1 we first extended our previous finding of elevated *FOXG1* mRNA expression in GBM by assessing levels of FOXG1 protein. FOXG1 protein is consistently and highly expressed across a set of nine independent patient-derived GNS cell lines when compared to NS cells (Fig. 1A). It is also increased in a mouse glioma-initiating cell line (Supplemental Fig. S1). SOX2 protein levels are high in both NS and GNS cells. OLIG2, a developmental TF often expressed in GBM, is more variably expressed between GNS lines (Fig. 1A).

High levels of FOXG1 in GNS cells might contribute to a modified chromatin landscape compared to karyotypically normal NS cells. To assess chromatin accessibility genome-wide in GNS and NS cells we performed ATAC-seq (Buenrostro et al., 2013). Seven independent human GNS lines (G7, G14, G19, G25, G26, G32, G144, G166, G179), and four human NS cell controls, were assayed in biological duplicate under proliferative culture conditions. Unsupervised clustering using the most variable sites across these libraries clearly separated GNS from NS cells (Fig. 1B). As expected, given patient heterogeneity, GNS cells had a greater diversity of chromatin profiles than NS cells. Interestingly, the regions identified as more accessible in GNS versus NS cells were enriched in the forkhead box motif and HMG box motif which are bound by FOX and SOX factors, respectively (Fig. 1C). These data suggest that increased FOXG1 protein levels and FOX/SOX enriched chromatin accessibility sites are a hallmark that distinguishes GNS cells from genetically normal NS cells.

Loss of FOXG1 sensitises NS cells to astrocyte differentiation cues

Mouse NS cells are a genetically and experimentally tractable model for interrogating self-renewal and differentiation commitment. Replacement of the growth factors EGF/FGF-2 with BMP4 results in prompt and uniform cell cycle exit and upregulation of astrocyte markers including Gfap and Aqp4 (Fig. 2A-C) (Conti et al. 2005). We used this culture system to explore the specific and shared functions of Foxg1 and Sox2.

Sox2 has previously been shown be essential for NS cell self-renewal *in vitro* (Gómez-López, et al, 2011). To test whether Foxg1 is required for *in vitro* self-renewal of NS cells we derived a new NS cell line (termed FF) from the subventricular zone of a previously reported adult *Foxg1*$^{flox/flox}$ mouse (Miyoshi and Fishell, 2012) (Fig. S2A). Transient transfection with a Cre expression plasmid resulted in biallelic excision of the *Foxg1* coding locus. Monitoring of the Foxg1 ablated cells over many passages – using a GFP reporter of Cre excision – suggested there was no proliferation deficit (Fig. S2B). Indeed, we could readily establish clonal *Foxg1* mutant NS cell lines (Fig. 2D). The mutant cells demonstrated no difference in proliferation or marker expression when grown in EGF/FGF-2; they also retained astrocyte differentiation potential (Fig. S2B-C). However, in response to a combination of BMP4 and reduced amounts of EGF/FGF-2, *Foxg1*$^{-/-}$ cells showed an increased propensity to exit cycle and differentiate (Fig. 2E). These data suggest that Foxg1 is dispensable for the maintenance of continued NS cell proliferation *in vitro*. It may be required instead to protect cells from differentiation commitment.

Overexpression of FOXG1 and SOX2 in adult NS cells suppresses BMP-induced astrocyte differentiation

The high levels of FOXG1 and SOX2 in GBM stem cells may underlie the failure of differentiation commitment and unconstrained self-renewal associated with these malignancies (Carén et al., 2015). To test the consequences of increased FOXG1 and SOX2, we transfected genetically normal adult subependymal zone (SEZ)-derived mouse NS cell cultures (ANS4) with a stably integrating PiggyBac transposon plasmid carrying a tetracycline-inducible *FOXG1-2A-SOX2* expression cassette (Fig. 2F). Clonal NS cell lines were generated that responded to doxycycline (Dox) treatment by increasing expression of FOXG1 and SOX2 mRNAs in a dose-dependent manner (Fig. 2F-H). We used the human FOXG1 and SOX2 coding sequence, as the major goal was to uncover their roles in human GBM and these are each ~97% identical at the protein level to their mouse homologs, with 100% homology in the DNA binding domains (Fig. S2D). In parallel, we established inducible lines expressing FOXG1 or SOX2 individually, termed F6 and S15, respectively (Fig. S2E-F). FOXG1 was expressed as a fusion protein with a V5 epitope tag that enabled monitoring of transgene expression.

We cultured FS3, F6, and S15 cells in self-renewal media (EGF/FGF-2) plus BMP4, with or without Dox. Under these conditions, parental ANS4 cells adopt an astrocyte morphology and stop proliferating. Dox-induced expression of either FOXG1 or SOX2 alone had little effect on astrocyte differentiation and cells did not proliferate. However, co-expression of both factors restricted the differentiation response, and cultures remained proliferative (Fig. 2I-J). These data indicate that overexpression of FOXG1 and SOX2 in combination can attenuate the cytostatic effects of BMP-induced astrocyte differentiation.

Overexpression of FOXG1 and SOX2 in post-mitotic astrocytes triggers de-differentiation to a proliferative NS cell-like state

We next explored the functional consequences of forced expression of FOXG1 and SOX2 in differentiating astrocytes. A quantitative *in vitro* colony forming assay was developed to determine if these factors can trigger cells to re-enter cell cycle and de-differentiate to the proliferative NS cell state (Fig. 3A). As a positive control we used a previously reported glioma-initiating mouse NS cell line, IENS (*Ink4a/ARF* deletion; EGFRvIII overexpression) (Bachoo et al., 2002; Bruggeman et al., 2007). IENS cells express FOXG1 at high levels relative to normal NS cells (ANS4) and are highly malignant on transplantation (Supplemental Fig. S1B).

When parental ANS4 cells are plated at low density (10 cells/mm^2) and cultured for 24 hours in the presence BMP4 but without the growth factors EGF/FGF-2, all cells undergo astrocyte differentiation and are subsequently unable to re-enter cell cycle when re-exposed to self-renewal media, as assessed by EdU incorporation; i.e. they are post-mitotic and growth factor unresponsive (Fig. 3B and S3A). When returned to self-renewal conditions glioma-initiating IENS cells form scattered proliferating NS cell-like colonies, consistent with a suppression of BMP-induced differentiation (Fig. 3C).

Dox-induced expression of exogenous FOXG1 and SOX2 in the growth factor unresponsive and post-mitotic astrocytes (BMP-treated, FS3 cells) resulted in dose-dependent colony formation (Fig. 3C), whereas the no Dox-treated controls failed to form colonies. The colonies that emerged in Dox-treated plates were rapidly cycling and comprised Nestin-high, Gfap-low cells with a characteristic NS cell morphology (Fig. 3D). FOXG1/SOX2-induced colonies were typically similar in size to control NS

cell colonies (data not shown), and inspection of time-lapse imaging of de-differentiation revealed doubling times of ~24 hours, which is comparable to parental NS cells and suggests cells rapidly adopt a highly proliferative NS cell-like phenotype (Fig. S3B and Supplemental Movie 1). Transcriptome profiling of these cells by RNA-seq identified expression changes compatible with de-differentiation and reacquisition of many features of the untreated parental cells grown in EGF/FGF-2 (Fig. 3E), such as differentiation potential (Fig. 3F). The de-differentiated cells continued to divide upon Dox withdrawal and could be serially passaged; they exhibited a morphology, proliferation rates and marker expression similar to the parental FS3 cells (Supplemental Fig. S3C-E). They also remained BMP4-responsive and activate Gfap (Supplemental Fig. S3F).

To exclude the possibility that FOXG1/SOX2-induced astrocyte de-differentiation was limited to *in vitro* generated astrocytes, we next introduced the TET-*FOXG1-2A-SOX2* transgene into freshly isolated mouse astrocytes (Fig. 3G). Induction of FOXG1 and SOX2 in primary astrocytes contributed to a significant increase in NS cell-like colonies when cells were transferred into self-renewal media. We conclude that overexpression of FOXG1 and SOX2 in astrocytes reverses differentiation, and is sufficient to drive cells to enter cell cycle and acquire a proliferative NS cell identity (Fig. 3H).

ChIP-seq identifies FOXG1 binding at core cell cycle and methyltransferase target genes

The *in vitro* de-differentiation assay provided a tractable system to define transcriptional target genes through which FOXG1 and SOX2 operate. Sox2 target

genes in mouse neural progenitor cells have been previously defined using ChIP-seq (Lodato et al., 2013). Identification of FOXG1 targets has been hindered by the limitations of available native antibodies. To overcome this, we performed ChIP-seq in NS cells constitutively expressing the V5 epitope-tagged version of FOXG1, which remained functional in our earlier dedifferentiation assays (Fig. 3). Two independent NS cell lines constitutively overexpressing FOXG1-V5 were generated from ANS4 and an independent primary adult SVZ-derived NS cell line. From the V5 ChIP-seq we identified 6897 high confidence binding sites shared between these cell lines, and motif enrichment analysis confirmed the canonical forkhead motif to be most significantly enriched (Fig. 4A). We also found many other neurodevelopmental lineage-affiliated TF motifs enriched at these sites, including: bHLH, HMG box (the SOX family binding motif) and CTF/NF1 factors (Fig. 4A). These are bound by TFs recognised as key components of the core circuit of self-renewal in NS cells (Mateo et al., 2015). Genes associated with these peaks were enriched in several notable Gene Ontology (GO) categories, including: Notch and TGF-beta signaling, stem cell maintenance and methyltransferase/histone methyltransferase function (Fig. S4). Mitochondrial GO terms were also identified, consistent with reports of a role for FoxG1 in the regulation of mitochondrial function (Pancrazi et al., 2015).

We next examined the intersection of newly defined FOXG1 peaks with the 16683 sites previously reported as bound by Sox2 in cultured mouse neural progenitors (Lodato et al., 2013). There was a substantial overlap, with 3856 of the 6897 FOXG1 peaks also represented in the Sox2 dataset (Fig. 4B). The associated set of genes is strongly enriched for GO categories including: Notch signaling, histone methyltransferase complex, mitotic cell cycle checkpoint, and stem cell maintenance (Fig. 4C). This is consistent with the functional consequences of overexpression of

FOXG1/SOX2 – namely, cell cycle re-entry and de-differentiation – and suggests both factors may play a role in controlling these processes.

Binding of a TF alone does not constitute evidence of a functional role in regulating the candidate target gene. RNA-seq was therefore performed in order to identify a subset of candidate FOXG1/SOX2 regulated loci (Fig. 4D). As anticipated, BMP exposure rapidly led to downregulation of *Nestin* expression and upregulation of the astrocyte markers *Aqp4* and *Gfap*. Of note, FOXG1/SOX2 bound targets that showed altered expression 4 days after Dox treatment and return to self-renewal media (EGF/FGF-2) included core regulators of cell cycle (*Plk1, Foxo3, Mycn)* and epigenetic processes (*Dnmt1* and *Tet3)* (Fig. 4D). *Foxo3* expression was one of the most significantly upregulated genes after 24 hr of BMP treatment, and was downregulated upon treatment with Dox and exposure to EGF/FGF-2. Foxo3 is a well-established negative regulator of cell proliferation downstream of the PI3K signaling pathway. FOXG1/SOX2 bound regions included the proximal promoter and a conserved intronic element harboring multiple motifs for SOX and FOX (Fig. 5C). We therefore pursued this as a candidate functionally important target.

Transcriptional repression of *Foxo3* by FOXG1/SOX2 removes a barrier to astrocyte cell cycle re-entry

Foxo3 has an established role in NS cell homeostasis and quiescence (Webb et al., 2013), and a recent study suggests it is directly regulated by Foxg1 (Vezzali et al., 2016). Our own RNA-seq data indicated a rapid upregulation of *Foxo3* mRNA following BMP-induced astrocyte differentiation (Fig. 4D). Levels of *Foxo3* mRNA are reduced following addition of Dox and a switch to NS cell media (Figs. 4D and 5A).

ICC for Foxo3 protein confirmed upregulation and nuclear translocation following BMP treatment (Fig. 5B). ChIP-seq data indicated binding of both FOXG1 and SOX2 at a highly conserved intronic element (CIE) within *Foxo3* (Fig. 5C). This region contains multiple repeats of the sequence AAACA, which comprises part of binding motifs for FOX and SOX transcription factors in NS cells (Lodato et al., 2013).

To directly test the functional significance of binding at the *Foxo3* CIE we took advantage of CRISPR/Cas9 genome editing, which we have optimized for mouse and human NS cells (Bressan et al., 2017). Using a pair of guide RNAs (gRNAs) we deleted the 780 bp Foxg1/Sox2-bound CIE in FOXG1/SOX2 overexpressing FS3 cells (Fig. 5C). Sub-clones were identified in which both alleles were disrupted (Fig. 5D). Deletion of this element led to increased levels of *Foxo3* mRNA expression under self-renewal conditions (EGF/FGF-2) (Fig. 5E), and proliferation of this line was marginally slower (data not shown). Importantly, these cells were now unable to undergo de-differentiation in response to FOXG1/SOX2 overexpression (Fig. 5F). We surmise that this regulatory element is critical in enabling FOXG1/SOX2 to repress *Foxo3* expression, thereby removing a critical blockade to cell cycle re-entry.

To confirm the potential relevance of these findings to human GBM, we performed ChIP-seq for FOXG1 in four independent human GNS cell lines (G7, G14, G25 and G166) using an antibody against endogenous FOXG1. Although less specific than V5 ChIP, we identified a total of 7499 peaks and noted strong enrichment for the forkhead box and related motifs (Fig. S5A). These data showed that FOXG1 was bound to the *FOXO3* CIE (Fig. S5B).

Reacquisition of the proliferative NS cell state can be achieved by combined loss of *Foxo3* and alterations to DNA methylation

To test the consequences of *Foxo3* deletion, we excised exon 2 of *Foxo3* in FS3 cells using CRISPR/Cas9-assisted gene targeting (Bressan et al., 2017). Biallelic mutant lines were generated through simultaneous replacement of one *Foxo3* allele with an EF1a-Puromycin resistance cassette and insertion-deletion (indel) mutations on the remaining allele (Fig. S5C). Foxo3 protein was undetectable in a clonal line that contained a frameshift indel mutation and generated a nonsense product (FOD3; Fig. 5G). These FOD3 *Foxo3*$^{-/-}$ mutant cells retained a similar responsiveness to BMP treatment as their parental cells, with concomitant upregulation of astrocyte markers including Gfap and acquisition of the characteristic morphology (data not shown). However, in contrast to parental controls which exited cell cycle, *Foxo3* mutant cells proliferated slowly on re-exposure to EGF/FGF-2 without Dox (doubling time of ~6 days; Fig. 5H). Thus, *Foxo3* ablation sensitises astrocytes to growth factors and relieves a barrier to cell cycle re-entry. Importantly, however, these cells did not fully de-differentiate and retained Gfap expression (Fig. 5H-J). They remained slow-cycling. We conclude that cell cycle entry and differentiation status are uncoupled in the context of *Foxo3* deletion. Additional target genes are therefore required to trigger de-differentiation and rapid proliferation.

We previously reported that human GBM stem cells fail to undergo terminal differentiation commitment and have aberrant DNA methylation patterns in response to BMP treatment (Carén et al., 2015). Shared transcriptional targets of FOXG1/SOX2 included several regulators of DNA and histone methylation. These genes represent clear candidates that might be involved in destabilizing astrocyte differentiation. Inhibition of DNA methyltransferase (Dnmt) activity by the nucleoside analogue 5-

azacytidine (Aza) has been reported to facilitate iPS cell reprogramming (Mikkelsen et al., 2008). We therefore hypothesized that Dnmt inhibition by 5-Aza might enable de-differentiation by interfering with establishment or maintenance of the DNA methylation profile in differentiating astrocytes. Indeed, either 5-Aza or ascorbic acid (a co-factor for Tet proteins), could trigger increased proliferation in populations of *Foxo3* mutant astrocytes (Fig. S5D). This was quantified for 5-Aza using colony formation assays for the slow cycling BMP-treated Foxo3 mutants (FOD3). Strikingly, the combination of Aza treatment with *Foxo3* deletion resulted in emergence of rapid-cycling populations forming similar numbers of Nestin-positive colonies to the Dox-treated FS3 cultures (Fig. 5H-J). Thus, Aza in combination with loss of *Foxo3* can phenocopy the effects of FOXG1/SOX2 induction. Resetting of DNA methylation patterns that are acquired during astrocyte differentiation may therefore be a critical feature of FOXG1/SOX2 reprogramming activity.

FOXG1 overexpression affects multiple regulators of DNA methylation to facilitate de-differentiation

We next investigated the effect of forced expression of higher levels of FOXG1 or SOX2 alone using the F6 and S15 lines, respectively (Fig. S2E-F). Each of these lines enabled higher levels of each individual factor to be expressed in differentiating astrocytes. High levels of induction of FOXG1 alone, but not SOX2, was sufficient to drive efficient colony formation in two independent FOXG1 inducible lines (F6 and F11) (Fig. 6A-B). The resulting de-differentiated cells displayed morphology, proliferation kinetics and marker expression similar to the parental line and responded to BMP-induced differentiation (Fig. S6A and S6C-E). RNA-seq confirmed that these cultures were re-acquiring NS cell-like transcriptional signatures and many of the

activated genes included FOXG1/SOX2 bound genes (Fig. 6C). We confirmed by RNA-seq and qRT-PCR that there is a significant increase in expression of *Dnmt1*, *Dnmt3b* and *Tet3* following increased FOXG1 expression (Fig. 6D and S6B). Thus, the excessively high levels of expression of FOXG1 in GBM may specifically operate in limiting differentiation (Fig. 6).

DNA methylation changes at polycomb target genes, including *Foxo3,* occur during astrocyte differentiation

To define the DNA methylation changes that accompany BMP-induced astrocyte differentiation we performed reduced representation bilsulfite sequencing (RRBS). Analysis of the resulting methylation profiles identified a total of 3231 significantly Differentially Methylated Regions (DMRs) after 24 hr or 10 days of BMP-induced differentiation (756 with reduced methylation and 2475 with increased methylation). These DMRs where significantly enriched near developmental TFs (Fig. S6F). Developmental TFs are known to be regulated by polycomb repressive complexes; indeed, BMP-induced differentiation DMRs were enriched near polycomb repressive complex target genes previously reported in mouse NS cells, embryonic stem cells and brain (Fig. 6E) (Meissner et al., 2008). This included methylation changes at the promoter of *Foxo3* close to a Foxg1 binding site (Fig. 6F). These analyses suggest that DNA methylation changes occur at developmental TFs during astrocyte differentiation and that FOXG1 may help in reconfiguring these during de-differentiation, via its control of multiple regulators of DNA methylation.

Genetic ablation of *FOXG1* in human GNS cells does not affect *in vitro* proliferation but *SOX2* is essential

Previous studies using shRNA knockdown of FOXG1 have suggested an important role in promoting tumour growth (Verginelli et al., 2013). CRISPR/Cas9 provides new opportunities for decisive functional genetic studies in primary human GBM stem cells. Using recently optimised protocols (Bressan et al., 2017), we next performed gene targeting via homologous recombination to delete *FOXG1* in human primary GNS cells (G7) (Fig. S7A). One of the resulting clonal lines (G7-A1) harboured a 23 bp frameshift insertion at the second allele and demonstrated loss of FOXG1 protein by immunoblotting (Fig. 7A and S7A). In contrast to previously reported findings using tumour sphere models, we found no discernible effect of FOXG1 ablation on proliferation rates of GNS cells *in vitro* (Fig. 7B).

We next compared the FOXG1 loss-of-function phenotype with SOX2 loss in G7 cells. Previous studies have suggested that Sox2 is required for self-renewal of forebrain NS cells: homozygous knockout by conditional deletion or CRISPR/Cas9 targeting is incompatible with colony formation (Bressan et al., 2017; Gómez-López et al., 2011). Here, CRISPR/Cas9 was used to mutate the single coding exon of *SOX2* (Fig. S7B). We were unable to recover expandable SOX2 mutant clones, suggesting these may have a proliferation defect. The proportion of SOX2 negative cells were tracked in the primary transfected population over time by ICC (Fig. S7C-E). ~25% of mutant cells were detectable in the transfected population at day 7; however, by day 14 and day 42 this subpopulation had dropped to ~18% and <1% of the population, respectively. Co-culture with the non-deleted wild-type cells clearly could not rescue the proliferation defect. We conclude that loss of *SOX2* ablates the proliferative

capacity of patient-derived GBM cells in a cell autonomous manner. This contrasts with *FOXG*1, which is dispensable for *in vitro* NS cell proliferation.

FOXG1 **mutant human GNS cells are sensitised to cytostatic signals *in vivo* and upregulate FOXO3**

To test the consequences of FOXG1 loss *in vivo* we transplanted cells orthotopically into the brains of immunocompromised mice. A GFP reporter construct was inserted at the safe harbour *AAVS1* locus, in both parental control cells and the *FOXG1*$^{-/-}$ clone to enable monitoring of cells following xenotransplantation. Consistent with the previously reported shRNA knockdown results (Verginelli et al., 2013), we saw a failure of the *FOXG1*$^{-/-}$ G7-A cells to form tumours on transplantation into immunocompromised mice (Fig. 7C; n=4). We hypothesised that FOXG1 is able to protect cells from pro-differentiation signals that would trigger exit from the cell cycle *in vivo*.

Our findings in mouse NS cells suggested that FOXG1 operates in part by helping repress *FOXO3* and this could be a key effector of its function by limiting astrocyte differentiation. We therefore assessed expression of GFAP and FOXO3 in the FOXG1 knockout cells following transplantation *in vivo*. The transplanted cells were present at the injection site and these were found to express high levels of GFAP and FOXO3 and low levels of Ki67 compared to wild type controls. They also, displayed morphological features of differentiated ‘star shaped’ astrocytes (Fig. 7D-H; n=4). This indicates that FOXG1 is required in GBM stem cells to sustain GNS cell growth *in vivo.* In conclusion, we find that SOX2 is essential for continued proliferation of GBM stem cells, while FOXG1 is not. However, increased levels of FOXG1

safeguard the stem cell state from pro-differentiation cues encountered outside the endogenous SVZ niche. This restriction of differentiation commitment is mediated at least in part through repression of negative regulators of proliferation such as *FOXO3.* (Fig. 7I).

Discussion

There are important conceptual and mechanistic similarities between cellular transformation in human cancers and cellular reprogramming (Suvà et al., 2013). FOXG1 and SOX2 are key regulators of forebrain neural progenitor fate and are known reprogramming factors (Lujan et al., 2012). Here we have demonstrated that high FOXG1 and SOX2 levels, a consistent feature of GNS cells, are functionally important in driving a highly proliferative, growth factor responsive, radial glia-like NS cell state. These master regulators operate through transcriptional control of various stem cell-associated pathways, most notably cell cycle and epigenetic regulators. Cancer stem cells therefore deploy overexpression of key lineage-affiliated TFs as a mechanism to fuel their self-renewal the same strategy used by stem cell biologists in experimental reprogramming.

FOXG1 is consistently upregulated across all GNS cells we assessed. Using ATAC-seq profiling of human GNS and NS cells, we identified an enrichment of open regions containing many neurodevelopmental TF motifs, including binding sites of SOX and FOX transcription factor families. This supported our hypothesis that increased levels of FOXG1 and SOX2 might be important in driving GBM cell self-renewal and is consistent with the known roles of these factors during development of the mammalian forebrain (Xuan et al., 1995).

We initially explored Foxg1 loss of function using a new conditional NS cell line. Mutant cells become sensitized to differentiation cues, but surprisingly, there was no proliferative defect *in vitro*. This contrasts with loss of Sox2, which has previously been shown to be a critical factor for proliferation of mouse NS cells. This suggested to us that the gain of function phenotype for Foxg1 is more critical, and its role might be specifically in limiting terminal differentiation commitment or driving de-differentiation.

A quantitative colony formation assay was developed to explore the consequences of increased expression of human FOXG1 and SOX2 in de-differentiating astrocytes, thereby mimicking the increased levels of FOXG1 seen in GBMs. We didn't observe increased levels of SOX2 protein in GNS cells, compared to NS cells. However, unlike FOXG1, SOX2 is amplified in GBM. It is possible that the levels of SOX2 in NS cells are already saturating in vitro. We find that NS cells plated at low density and treated with BMP4 for 24 hours exit cell cycle with acquisition of astrocyte morphology and markers. Quiescent NS cells *in vivo* express Gfap. So are we modelling the transition from quiescence to reactivation/proliferation, as opposed to terminal differentiation to de-differentiation? We believe this is less likely, as we could induce NS cell colony formation by FOXG1/SOX2 induction when using fresh primary postnatal astrocyte preparations. Furthermore, we have recently found low density BMP treated astrocytes have reduced levels of quiescent stem cell astrocyte markers (data not shown). A key functional criterion for distinguishing quiescent astrocytes and the differentiating astrocytes is that the latter cannot be driven into cycle when re-exposed to EGF/FGF-2. Thus, we view our assay as a de-differentiation response.

Our ChIP-seq data for FOXG1 and the intersection with SOX2-bound sites suggested that these factors have common target genes, including both important core cell cycle and epigenetic regulators. However, we have found no indication of physical interaction between SOX2 and FOXG1 using protein co-immunoprecipitation (data not shown). This is consistent with characterized SOX2 protein partner analysis in mouse NS cells (Engelen et al., 2011). Rather, it seems likely that FOXG1 and SOX2 are cooperating indirectly at the gene regulatory network level. Defining their shared transcriptional targets is therefore valuable and may help define new therapeutic targets.

Exposure to Dox and EGF/FGF-2 triggered a relatively rapid emergence of proliferating colonies, whether from NS cell-derived *in vitro* generated astrocytes, or astrocytes from primary cultures. Inspection of this response by time-lapse imaging together with the sizes of resulting colonies suggested that cell cycle re-entry was an early event. We recognize that multiple targets will contribute to the potency of FOXG1/SOX2 activity, and we searched for those candidates that might have a major contribution. Foxo3, which has an established role in NS cell homeostasis and quiescence, emerged as a functionally important transcriptional target of FOXG1/SOX2. This finding is consistent with Foxo3 as a transcriptional target of FOXG1 during telencephalic development (Vezzali et al., 2016). FOXO3 activity is also known to be affected by interaction with FOXG1 at the protein level (Seoane et al., 2004); FOXG1 therefore exerts a dual inhibition of FOXO3 activity, at the protein-protein level and through transcriptional suppression. We used CRISPR/Cas9 genetic ablation to confirm FOXG1 repression of *Foxo3* at the transcriptional level. Importantly, in the absence of the FoxG1-bound repressive element in the *Foxo3* intron, NS cells could no longer respond to Dox. Transcriptional repression of Foxo3 through this site may therefore be the primary mechanism of control by FoxG1, with the sequestration through protein-protein interaction being an added layer of regulatory control.

Foxo3 ablation removes a barrier to cell cycle re-entry; however, the mutant cells retained astrocyte morphology, high GFAP expression and displayed slow proliferation kinetics on restoration of growth factors following BMP treatment. Foxo3 repression alone is therefore insufficient to trigger full de-differentiation to an NS cell-like state. Additional targets must exist. Given the prominence of methyltransferase and histone methyltransferase complexes in Gene Ontology analysis of the FOXG1/SOX2 bound regions, we explored whether resetting of DNA methylation

patterns could remove a barrier to de-differentiation. This proved to be the case, as a short 24 hr pulse of a low dose of Aza (a nucleoside analogue which inhibits DNA methyltransferase activity) or ascorbic acid (co-factor of the TET family of enzymes which trigger DNA demethylation) was sufficient to stimulate rapid proliferation of *Foxo3* mutant cells. Thus, the effects of FOXG1/SOX2 overexpression can be phenocopied by removal of Foxo3 and reconfiguration of DNA methylation patterns. Multiple regulators of DNA methylation were bound by FOXG1, including Tet3, Dnmt3b and Dnmt1. These displayed changes in expression upon Dox treatment in FOXG1 alone overexpressing cells (F6).

DNA methylation profiling using RRBS identified significant methylation changes in astrocytes following 24 hr BMP4 treatment that were heavily enriched for polycomb target genes, including Foxo3. Unfortunately, as only a subpopulation of the cells undergo de-differentiation following re-exposure to growth factors and addition of Dox, we were unable to identify any significant changes in methylation after 4 days (data not shown). Future studies will require isolation/enrichment for the earliest de-differentiating cells to define the specific link between key sites of methylation changes and FOXG1 binding. Tet3 is a clear candidate that might impact the stability of the methylome in differentiating astrocytes. Our current data supports a model in which high levels of FOXG1/SOX2 have at least two complementary activities: stimulation of core cell cycle regulators and triggering of epigenetic resetting to drive post-mitotic astrocytes into the more immature radial glial-like NS cell state (Fig. 7I). Further definition of the downstream targets of these factors might uncover ‘druggable’ targets, and guide rational combination therapy strategies.

Not all astrocytes are able to respond to FOXG1/SOX2. It is possible that additional factors or signaling pathway manipulations could improve efficiency. There

might also be some stochastic element to triggering de-differentiation, as is the case with iPS cell reprogramming (Buganim et al., 2012). Other noteworthy annotated gene sets that we identified via ChIP-seq analysis included mitochondrial function, Notch and Wnt/Beta catenin signaling. Many of these have been implicated in the growth of GBMs and further studies will be needed to define whether these can enhance de-differentiation.

Using CRISPR/Cas9 gene targeting we were able to genetically ablate FOXG1 in primary human GBM stem cells. FOXG1 is dispensable for *in vitro* NS cell proliferation when cultured in adherent conditions with EGF/FGF-2. This seemingly contradicts previous shRNA knockdown studies that concluded FOXG1 is required to sustain proliferation (Verginelli et al., 2013). However, Verginelli et al. assayed proliferation using tumour spheres, a condition in which spontaneous differentiation can occur. Thus the discrepancy is likely explained by differences in culture regime. These findings are also consistent with the fact that we can routinely derive NS cell lines from different regions of the developing nervous system (midbrain, hindbrain, spinal cord) that express *FoxG1* neither *in vivo* nor *in vitro*. Thus FOXG1 is not an essential cell cycle driver in NS cells; rather, it is required to protect cells from pro-differentiation cues and can trigger the transition out of the non-proliferative state.

Previous studies have explored the core transcriptional circuits that might be exploited by GBM stem cells. A reprogramming cocktail incorporating SOX2, OLIG2 and POU3F2 has been used to reinstate tumorigenicity in 'differentiated' glioblastoma cells (Suvà et al. 2014) and this network was generated by focusing on TFs differentially expressed between GBM stem cells and serum-induced differentiating progeny. FOXG1 was not among the factors comprising the core transcriptional circuit identified in these studies. However, a recent study by the Barres laboratory (Zhang et

al., 2016) has identified genes differentially expressed betweeen immature fetal astrocytes from post-mitotic adult cortical astrocytes. FOXG1 is indeed one of the most differentially expressed genes (Fig. S7F). We speculate that upregulation of FOXG1 expression is a critical event in the emergence of GBM, occurring either early in tumorigenesis to produce primary glioblastoma, or later resulting in secondary transformation of a low grade glioma. In keeping with this, we have found variable FOXG1 expression in a panel of tumour lines derived from WHO Grade II and Grade III gliomas (data not shown).

In conclusion, we show that elevated FOXG1 plays a functionally important role in limiting differentiation commitment, whereas SOX2 is required to sustain NS and GNS cell proliferation. When co-expressed these two factors drive self-renewal and enforce a proliferative radial glial-like NS cell state. Although we find no evidence of a protein level interaction between these factors, they share multiple core cell cycle and epigenetic regulatory targets. Our findings highlight the increasing evidence in support of a critical role for neurodevelopmental transcription factors in driving unconstrained self-renewal in GBM.

Experimental procedures

Cell culture

Mouse and human neural stem (NS) and glioma neural stem (GNS) cell lines were derived from adult subventricular zone, fetal cortex or primary glioblastoma specimens as previously described (Conti et al. 2005; Sun et al. 2008). Established lines were cultured in serum-free basal medium supplemented with N2 and B27 (Life Technologies), laminin (Sigma, 1mg/ml) and growth factors EGF and FGF-2 (Peprotech, 10 ng/ml). Medium was changed every 3 days and cells split typically once per week after dissociation with Accutase solution (Sigma) and centrifugation.

BMP treatment comprised plating dissociated NS cells at low density (10 cells/mm^2) in medium supplemented with 10 ng/ml BMP4 (Peprotech) in place of EGF/FGF-2. After 24 hours this was replaced by standard growth medium containing EGF/FGF-2. Colonies were stained with ethidium bromide and visualized under UV light.

IENS cells, previously described (Bruggeman et al., 2007), were kindly provided by M. Van Lohuizen (NKA, Amsterdam). A table detailing the mouse NS cell line derivatives established here and a summary of their differentiation/de-differentiation characteristics is provided (Supplemental Table 1). Growth curves were generated using an IncuCyte live cell imaging system.

Primary mouse astrocyte cultures were prepared from the trypsin-digested cortical plate tissue of P3 mice cortices (strain MF1), according to established protocols (Schildge et al., 2013), including shake-off after one week to remove contaminating microglia and progenitor cells.

Derivation of stable transgenic and knockout cell lines

One million cells were transfected with the Amaxa Nucleofector system, using either the X005 pulse protocol (human cells) or T-030 protocol (mouse cells).

For inducible transgene overexpression, a total of 6 µg DNA was supplied comprising piggyBac transposase pBASE, pCAG-rtTA(Tet3G) and pDEST-TetOn vector in 1:1:2 ratios. For CRISPR targeting, guide RNAs (x2), targeting vector (where appropriate) and Cas9 nickase were transfected in a 1:1:1:2 ratio.

Cells were plated in 10 cm dishes, with doxycycyline added after 24 hours where appropriate, and selection commenced 48 hours post-transfection using blasticidin (5 µg/ml), puromycin (1 µg/ml) or hygromycin (100 µg/ml). Each of these antibiotics produced uniform cell death within 7 days in untransfected mock controls (both human NS and GNS cells).

G7 primary human GNS cells were transfected with Cas9 nickase, guide RNAs corresponding to the forkhead domain of the *FOXG1* locus, and a targeting vector comprising an EF1a-PURO antibiotic resistance cassette flanked by 1 kb homology arms specific for the locus.

Immunocytochemistry

Cells were washed with PBS and fixed using 4% paraformaldehyde for 10 min at room temperature. Samples were incubated overnight with primary antibodies in blocking solution (PBST +3% goat serum and 1% BSA) followed by incubation with appropriate secondary antibodies and 4',6-diamidino-2-phenylindole (DAPI). Images were obtained using the Zeiss Observer Z1 microscope and AxioVision software, or the PerkinElmer Operetta high content imaging system and Harmony software. Transplanted mice brains were harvested, sectioned into 30 µm slices using a

vibratome, stained using IHC as free-floating staining, and imaged using a Leica SP8 confocal microscope.

The following primary antibodies were used: Olig2 (1:100, Millipore), V5 tag (1:1000, eBioscience), Sox2 (1:50, R&D Systems), mNestin (DSHB, 1:10), hNestin (1:500, R&D Systems), FOXG1 (1:3, hybridoma clone 17B12), FOXO3 (1:800, CST), GFAP (1:1000, Sigma), S100 (1:100, DAKO), Stem121 (1:500, StemCells), BLBP (1:200, Santa Cruz) and Ki67 (1:500, Lab Vision). EdU incorporation assays were performed as previously described (Caren et al., 2015).

Western immunoblotting

Immunoblotting was performed using standard protocols. Antibodies were diluted in 5% milk powder in PBS triton 0.1%, and protein detection was carried out with HRP-coupled secondary antibodies and X-ray films. The following primary antibodies were used: FOXG1 (1:15, hybridoma clone 17B12), SOX2 (1:400, R&D Systems), OLIG2 (1:800, Millipore) GAPDH (1:1000; GenTex), and V5 tag (1:1000; eBioscience).

qRT-PCR and Low Density Arrays

RNA extraction was performed using the Qiagen RNeasy Plus Mini spin column kit, eluting in 50 µl RNase free water and using an additional DNase step. RNA concentration was determined using the Qubit RNA High Sensitivity kit (Life Technologies). Reverse transcription was performed using Invitrogen Superscript III kit according to manufacturers' instructions. TaqMan qPCR and TaqMan Low Density Array (TLDA) card assays were performed using TaqMan Universal PCR Master Mix and assays (Applied Biosystems) according to the manufacturer's guidelines. Results were normalised to the housekeeping gene, Gapdh. The following TaqMan assays were used: mGapdh (Mm99999915_g1), mFoxG1 (Mm02059886_s1), mFoxo3

(Mm01185722_m1), mGfap (Mm01253033_m1), mAqp4 (Mm00802131_m1), mS100b (Mm00485897_m1), mNestin (Mm00450205_m1), mOlig2 (Mm01210556_m1), mBlbp (Fabp7) (Mm00445225_m1), mSox2 (Mm03053810_s1), mDnmt1 (Mm01151063_m1), mDnmt3b (Mm01240113_m1), mTet3 (Mm00805756_m1) and hGAPDH (Hs02758991_g1).

RNA-seq library construction

RNA sequencing libraries were prepared from 100 ng mRNA extracted using Qiagen RNeasy kits. Library prep was conducted using NEBNext mRNA reagents (E6100) and multiplex indices for Illumina (E7335).

ChIP-seq library construction

Chromatin was prepared and immunoprecipitation undertaken according to protocols previously described (Hadjur et al., 2009). Sonication was performed in 0.7% SDS using a Diagenode Bioruptor (max power 30 seconds on, 30 seconds off, 45 minutes). Pulldown was undertaken using Dynabead protein G sepharose beads (Thermo Scientific) conjugated with 10 µl of ChIP-grade antibody (anti-FoxG1 Abcam Ab18259; anti-V5 Abcam Ab15828) diluted in 250 µl buffer.

ATAC-seq library construction

ATAC-seq libraries were prepared using Illumina Nextera reagents as described (Buenrostro et al., 2013), with PCR amplification and indexing using published sequencing adapter primer sequences supplied as oligonucleotides (Sigma) (Buenrostro et al., 2013).

ChIP-seq data analysis

Filtered read files were imported to the Galaxy web-based analysis portal. Within Galaxy, the files were parsed into Sanger FastQ format, then each read was truncated from 100 base pairs to 55 (base pairs 10-65 of the original read). The read files were each mapped to the mouse genome (mm10 assembly) using Bowtie conFig.d with default parameters. The resulting BAM alignment files were merged into a single file, and peak calling was performed using the MACS 2.0 algorithm. Galaxy was also used to determine motif enrichment (SeqPos Motif tool), and the Stanford Genomic Regions of Enrichment Annotations Tool (GREAT version 3.0.0) was used for target gene and ontology analysis.

ATAC-seq data analysis

ATAC-seq data was imported, normalised and compared as described previously (Carén et al, 2015), with the exception of motif analysis which was applied to GNS enriched loci using all accessible chromatin sequences as a control. Heatmaps were generated from CQN normalised data (Hansen et al., 2012) using the Euclidean distance metric and Ward's method for clustering the rows.

Reduced Representation Bisulfite Sequencing library preparation

gDNA was isolated from F6 cells using MasterPure complete DNA purification kit (Epicentre) from three independent experiments and concentrated with the TM-5 DNA Clean and Concentrator kit (Zymo Research) before being quantified by Qubit dsDNA BR assay and Nanodrop. 85 ng of each purified DNA sample was processed using the Ovation RRBS Methyl-Seq System kit (NuGEN Technologies). 0.5 ng of unmethylated phage λ DNA was spiked in to each sample to allow assessment of bisulfite-conversion efficiency. Briefly, the methylation-insensitive restriction enzyme

MspI was used to digest the gDNA and digested fragments were ligated to adapters. Adapter-ligated fragments were then repaired before bisulfite- conversion with the EZ DNA Methylation-Lightning Kit (Zymo Research). Bisulfite-treated adapter-ligated fragments were amplified by PCR (15 cycles) and purified using Agencourt RNAClean® XP beads. Libraries were quantified using the Qubit dsDNA HS assay and assessed for size and quality using the Agilent Bioanalyser DNA HS kit. Sequencing was performed using the NextSeq 500/550 High-Output v2 Kit (150 cycles) (Illumina) on the NextSeq 550 platform. Libraries were combined into equimolar pools and run across four flow cells. Library preparation and sequencing was performed at the Edinburgh Clinical Research Facility.

Intracranial xenotransplantation

Transplants were performed as described previously (Pollard et al., 2009). Briefly, we used a stereotaxic frame to inject 100K cells in 1 µl into the striatum of adult NSG immunocompromised mice (aged 4-8 weeks). Co-ordinates were 1 mm anterior and 2 mm lateral to the Bregma, and 2.5 mm deep.

Author Contributions

Conceptualization, H.B. and S.M.P; Methodology, P.B. H.B, R.B., S.Go., S.Ga, V.F, D.S.; Formal Analysis, H.B., E.J, D.S; Investigation, H.B., E.J., M.M., K.F., R.B., C.B., V.G., S.Go., S.Ga, C.E.; Writing – Original Draft, H.B, S.P.; Visualization, H.B., E.J., S.M.P; Supervision, S.M.P, P.B; Project Administration, H.B., S.M.P.; Funding Acquisition, H.B, P.B., S.M.P.

Acknowledgements

H.B was supported by a Wellcome Trust Clinician Research Training Fellowship. E.J. was supported by the BBSRC. M.M is supported by an EMBO training fellowship. K.F is supported by a studentship from Cancer Research UK (A19680). R.B.B is supported by a studentship from the Science Without Borders Program (CAPES, Brazil). DS is a Cancer Research UK Career Development Fellow (Ref: C47648/A20837) and work in his lab is also supported by an MRC University Grant to the MRC Human Genetics Unit. S.M.P is a Cancer research UK Senior Research Fellow (A17368). We thank Gillian Morrison and Keisuke Kaji for helpful comments on the manuscript. We thank Richard Clark at the Edinburgh Clinical Research Facility for conducting the RRBS and helpful discussion on its data analysis.

References

Alonso, M.M., Diez-Valle, R., Manterola, L., Rubio, A., Liu, D., Cortes-Santiago, N., Urquiza, L., Jauregi, P., Lopez de Munain, A., Sampron, N., Aramburu, A., Tejada-Solís, S., Vicente, C., Odero, M.D., Bandrés, E., García-Foncillas, J., Idoate, M.A., Lang, F.F., Fueyo, J., Gomez-Manzano, C., 2011. Genetic and epigenetic modifications of Sox2 contribute to the invasive phenotype of malignant gliomas. PLoS ONE 6, e26740. doi:10.1371/journal.pone.0026740

Arnold, K., Sarkar, A., Yram, M.A., Polo, J.M., Bronson, R., Sengupta, S., Seandel, M., Geijsen, N., Hochedlinger, K., 2011. Sox2(+) adult stem and progenitor cells are important for tissue regeneration and survival of mice. Cell Stem Cell 9, 317–329. doi:10.1016/j.stem.2011.09.001

Avilion, A.A., Nicolis, S.K., Pevny, L.H., Perez, L., Vivian, N., Lovell-Badge, R., 2003. Multipotent cell lineages in early mouse development depend on SOX2 function. Genes Dev. 17, 126–140. doi:10.1101/gad.224503

Bachoo, R.M., Maher, E.A., Ligon, K.L., Sharpless, N.E., Chan, S.S., You, M.J., Tang, Y., DeFrances, J., Stover, E., Weissleder, R., Rowitch, D.H., Louis, D.N., DePinho, R.A., 2002. Epidermal growth factor receptor andInk4a/Arf:Convergent mechanisms governing terminal differentiation and transformation along the neural stem cell to astrocyte axis. Cancer Cell 1, 269–277. doi:10.1016/S1535-6108(02)00046-6

Brennan, C.W., Verhaak, R.G.W., McKenna, A., Campos, B., Noushmehr, H., Salama, S.R., Zheng, S., Chakravarty, D., Sanborn, J.Z., Berman, S.H., Beroukhim, R., Bernard, B., Wu, C.-J., Genovese, G., Shmulevich, I., Barnholtz-Sloan, J., Zou, L., Vegesna, R., Shukla, S.A., Ciriello, G., Yung, W.K., Zhang, W., Sougnez, C., Mikkelsen, T., Aldape, K., Bigner, D.D., Van Meir, E.G., Prados, M., Sloan, A., Black, K.L., Eschbacher, J., Finocchiaro, G., Friedman, W., Andrews, D.W., Guha, A., Iacocca, M., O'Neill, B.P., Foltz, G., Myers, J., Weisenberger, D.J., Penny, R., Kucherlapati, R., Perou, C.M., Hayes, D.N., Gibbs, R., Marra, M., Mills, G.B., Lander, E., Spellman, P., Wilson, R., Sander, C., Weinstein, J., Meyerson, M., Gabriel, S., Laird, P.W., Haussler, D., Getz, G., Chin, L., Network, T.R., Benz, C., Barnholtz-Sloan, J., Barrett, W., Ostrom, Q., Wolinsky, Y., Black, K.L., Bose, B., Boulos, P.T., Boulos, M., Brown, J., Czerinski, C., Eppley, M., Iacocca, M., Kempista, T., Kitko, T., Koyfman, Y., Rabeno, B., Rastogi, P., Sugarman, M., Swanson, P., Yalamanchii, K., Otey, I.P., Liu, Y.S., Xiao, Y., Auman, J.T., Chen, P.-C., Hadjipanayis, A., Lee, E., Lee, S., Park, P.J., Seidman, J., Yang, L., Kucherlapati, R., Kalkanis, S., Poisson, L.M., Raghunathan, A., Scarpace, L., Bernard, B., Bressler, R., Eakin, A., Iype, L., Kreisberg, R.B., Leinonen, K., Reynolds, S., Rovira, H., Thorsson, V., Shmulevich, I., Annala, M.J., Penny, R., Paulauskis, J., Curley, E., Hatfield, M., Mallery, D., Morris, S., Shelton, T., Shelton, C., Sherman, M., Yena, P., Cuppini, L., Dimeco, F., Eoli, M., Maderna, E., Pollo, B., Saini, M., Balu, S., Hoadley, K.A., Li, L., Miller, C.R., Shi, Y., Topal, M.D., Wu, J., Dunn, G., Giannini, C., O'Neill, B.P., Aksoy, B.A., Antipin, Y., Borsu, L., Berman, S.H., Cerami, E., Chakravarty, D., Ciriello, G., Gao, J., Gross, B., Jacobsen, A., Ladanyi, M., Lash, A., Liang, Y., Reva, B., Sander, C., Schultz, N., Shen, R., Socci, N.D., Viale, A., Ferguson, M.L., Chen, Q.-R., Demchok, J.A., Dillon, L.A.L., Shaw, K.R.M., Sheth, M., Tarnuzzer, R., Wang, Z., Yang, L., Davidsen, T., Guyer, M.S., Ozenberger, B.A., Sofia, H.J., Bergsten, J., Eckman, J., Harr, J., Myers, J., Smith, C., Tucker, K., Winemiller, C., Zach, L.A., Ljubimova, J.Y., Eley, G., Ayala, B., Jensen, M.A., Kahn, A., Pihl, T.D., Pot, D.A., Wan, Y., Eschbacher, J., Foltz, G., Hansen, N., Hothi, P., Lin, B., Shah, N., Yoon, J.-G.,

Lau, C., Berens, M., Ardlie, K., Beroukhim, R., Carter, S.L., Cherniack, A.D., Noble, M., Cho, J., Cibulskis, K., DiCara, D., Frazer, S., Gabriel, S.B., Gehlenborg, N., Gentry, J., Heiman, D., Kim, J., Jing, R., Lander, E.S., Lawrence, M., Lin, P., Mallard, W., Onofrio, R.C., Saksena, G., Schumacher, S., Sougnez, C., Stojanov, P., Tabak, B., Voet, D., Zhang, H., Zou, L., Dees, N.N., Ding, L., Fulton, L.L., Fulton, R.S., Kanchi, K.-L., Mardis, E.R., Wilson, R.K., Baylin, S.B., Andrews, D.W., Harshyne, L., Cohen, M.L., Devine, K., Sloan, A.E., VandenBerg, S.R., Berger, M.S., Carlin, D., Craft, B., Ellrott, K., Goldman, M., Goldstein, T., Grifford, M., Haussler, D., Ma, S., Ng, S., Salama, S.R., Sanborn, J.Z., Stuart, J., Swatloski, T., Waltman, P., Zhu, J., Foss, R., Frentzen, B., Friedman, W., McTiernan, R., Yachnis, A., Zheng, S., Vegesna, R., Mao, Y., Akbani, R., Bogler, O., Fuller, G.N., Liu, W., Liu, Y., Lu, Y., Mills, G., Protopopov, A., Ren, X., Sun, Y., Wu, C.-J., Yung, W.K.A., Zhang, J., Chen, K., Weinstein, J.N., Noushmehr, H., Weisenberger, D.J., Bootwalla, M.S., Lai, P.H., Triche, T.J., Jr, Van Den Berg, D.J., Laird, P.W., Gutmann, D.H., Lehman, N.L., VanMeir, E.G., Brat, D., Olson, J.J., Mastrogianakis, G.M., Devi, N.S., Zhang, Z., Bigner, D., Lipp, E., McLendon, R., 2013. The Somatic Genomic Landscape of Glioblastoma. Cell 155, 462–477. doi:10.1016/j.cell.2013.09.034

Bressan, R.B., Dewari, P.S., Kalantzaki, M., Gangoso, E., Matjusaitis, M., Garcia-Diaz, C., Blin, C., Grant, V., Bulstrode, H., Gogolok, S., Skarnes, W.C., Pollard, S.M., 2017. Efficient CRISPR/Cas9-assisted gene targeting enables rapid and precise genetic manipulation of mammalian neural stem cells. Development dev.140855–67. doi:10.1242/dev.140855

Bruggeman, S.W.M., Hulsman, D., Tanger, E., Buckle, T., Blom, M., Zevenhoven, J., van Tellingen, O., van Lohuizen, M., 2007. Bmi1 controls tumor development in an Ink4a/Arf-independent manner in a mouse model for glioma. Cancer Cell 12, 328–341. doi:10.1016/j.ccr.2007.08.032

Buenrostro, J.D., Giresi, P.G., Zaba, L.C., Chang, H.Y., Greenleaf, W.J., 2013. Transposition of native chromatin for fast and sensitive epigenomic profiling of open chromatin, DNA-binding proteins and nucleosome position. Nat Methods 10, 1213–1218. doi:10.1038/nmeth.2688

Buganim, Y., Faddah, D.A., Cheng, A.W., Itskovich, E., Markoulaki, S., Ganz, K., Klemm, S.L., van Oudenaarden, A., Jaenisch, R., 2012. Single-Cell Expression Analyses during Cellular Reprogramming Reveal an Early Stochastic and a Late Hierarchic Phase. Cell 150, 1209–1222. doi:10.1016/j.cell.2012.08.023

Carén, H., Stricker, S.H., Bulstrode, H., Gagrica, S., Johnstone, E., Bartlett, T.E., Feber, A., Wilson, G., Teschendorff, A.E., Bertone, P., Beck, S., Pollard, S.M., 2015. Glioblastoma Stem Cells Respond to Differentiation Cues but Fail to Undergo Commitment and Terminal Cell-Cycle Arrest. Stem Cell Reports 1–14. doi:10.1016/j.stemcr.2015.09.014

Engelen, E., Akinci, U., Bryne, J.C., Hou, J., Gontan, C., Moen, M., Szumska, D., Kockx, C., van Ijcken, W., Dekkers, D.H.W., Demmers, J., Rijkers, E.-J., Bhattacharya, S., Philipsen, S., Pevny, L.H., Grosveld, F.G., Rottier, R.J., Lenhard, B., Poot, R.A., 2011. Sox2 cooperates with Chd7 to regulate genes that are mutated in human syndromes. Nat Genet 43, 607–611. doi:10.1038/ng.825

Engström, P.G., Tommei, D., Stricker, S.H., Ender, C., Pollard, S.M., Bertone, P., 2012. Digital transcriptome profiling of normal and glioblastoma-derived neural stem cells identifies genes associated with patient survival. Genome Med 4, 76. doi:10.1186/gm377

Gangemi, R.M.R., Griffero, F., Marubbi, D., Perera, M., Capra, M.C., Malatesta, P., Ravetti, G.L., Zona, G.L., Daga, A., Corte, G., 2009. SOX2 silencing in glioblastoma tumor-initiating cells causes stop of proliferation and loss of

tumorigenicity. Stem Cells 27, 40–48. doi:10.1634/stemcells.2008-0493
Gómez-López, S., Wiskow, O., Favaro, R., Nicolis, S.K., Price, D.J., Pollard, S.M., Smith, A., 2011. Sox2 and Pax6 maintain the proliferative and developmental potential of gliogenic neural stem cells In vitro. Glia 59, 1588–1599. doi:10.1002/glia.21201
Kishi, M., Mizuseki, K., Sasai, N., Yamazaki, H., Shiota, K., Nakanishi, S., Sasai, Y., 2000. Requirement of Sox2-mediated signaling for differentiation of early Xenopus neuroectoderm. Development 127, 791–800.
Liu, F., Hon, G.C., Villa, G.R., Turner, K.M., Ikegami, S., Yang, H., Ye, Z., Bin Li, Kuan, S., Lee, A.Y., Zanca, C., Wei, B., Lucey, G., Jenkins, D., Zhang, W., Barr, C.L., Furnari, F.B., Cloughesy, T.F., Yong, W.H., Gahman, T.C., Shiau, A.K., Cavenee, W.K., Ren, B., Mischel, P.S., 2015. EGFR Mutation Promotes Glioblastoma through Epigenome and Transcription Factor Network Remodeling. Molecular Cell 60, 307–318. doi:10.1016/j.molcel.2015.09.002
Lodato, M.A., Ng, C.W., Wamstad, J.A., Cheng, A.W., Thai, K.K., Fraenkel, E., Jaenisch, R., Boyer, L.A., 2013. SOX2 co-occupies distal enhancer elements with distinct POU factors in ESCs and NPCs to specify cell state. PLoS Genet. 9, e1003288. doi:10.1371/journal.pgen.1003288
Lujan, E., Chanda, S., Ahlenius, H., Südhof, T.C., Wernig, M., 2012. Direct conversion of mouse fibroblasts to self-renewing, tripotent neural precursor cells. Proc. Natl. Acad. Sci. U.S.A. 109, 2527–2532. doi:10.1073/pnas.1121003109/-/DCSupplemental
Martynoga, B., Morrison, H., Price, D.J., Mason, J.O., 2005. Foxg1 is required for specification of ventral telencephalon and region-specific regulation of dorsal telencephalic precursor proliferation and apoptosis. Dev. Biol. 283, 113–127. doi:10.1016/j.ydbio.2005.04.005
Mateo, J.L., van den Berg, D.L.C., Haeussler, M., Drechsel, D., Gaber, Z.B., Castro, D.S., Robson, P., Crawford, G.E., Flicek, P., Ettwiller, L., Wittbrodt, J., Guillemot, F., Ben Martynoga, 2015. Characterization of the neural stem cell gene regulatory network identifies OLIG2 as a multifunctional regulator of self-renewal. Genome Research 25, 41–56. doi:10.1101/gr.173435.114
Mencarelli, M.A., Spanhol-Rosseto, A., Artuso, R., Rondinella, D., De Filippis, R., Bahi-Buisson, N., Nectoux, J., Rubinsztajn, R., Bienvenu, T., Moncla, A., Chabrol, B., Villard, L., Krumina, Z., Armstrong, J., Roche, A., Pineda, M., Gak, E., Mari, F., Ariani, F., Renieri, A., 2010. Novel FOXG1 mutations associated with the congenital variant of Rett syndrome. Journal of Medical Genetics 47, 49–53. doi:10.1136/jmg.2009.067884
Meissner A, Mikkelsen TS, Gu H, Wernig M, Hanna J, Sivachenko A, Zhang X, Bernstein BE, Nusbaum C, Jaffe DB, et al.: Genome-scale DNA methylation maps of pluripotent and differentiated cells. *Nature* 2008, 454:766–770.
Mikkelsen, T.S., Hanna, J., Zhang, X., Ku, M., Wernig, M., Schorderet, P., Bernstein, B.E., Jaenisch, R., Lander, E.S., Meissner, A., 2008. Dissecting direct reprogramming through integrative genomic analysis. Nature 454, 49–55. doi:10.1038/nature07056
Miyoshi, G., Fishell, G., 2012. Dynamic FoxG1 Expression Coordinates the Integration of Multipolar Pyramidal Neuron Precursors into the Cortical Plate. Neuron 74, 1045–1058. doi:10.1016/j.neuron.2012.04.025
Pancrazi, L., Di Benedetto, G., Colombaioni, L., Sala, Della, G., Testa, G., Olimpico, F., Reyes, A., Zeviani, M., Pozzan, T., Costa, M., 2015. Foxg1 localizes to mitochondria and coordinates cell differentiation and bioenergetics. Proc. Natl. Acad. Sci. U.S.A. 112, 13910–13915. doi:10.1073/pnas.1515190112

Patel, A.P., Tirosh, I., Trombetta, J.J., Shalek, A.K., Gillespie, S.M., Wakimoto, H., Cahill, D.P., Nahed, B.V., Curry, W.T., Martuza, R.L., Louis, D.N., Rozenblatt-Rosen, O., Suvà, M.L., Regev, A., Bernstein, B.E., 2014. Single-cell RNA-seq highlights intratumoral heterogeneity in primary glioblastoma. Science 344, 1396–1401. doi:10.1126/science.1254257

Rheinbay, E., Suvà, M.L., Gillespie, S.M., Wakimoto, H., Patel, A.P., Shahid, M., Oksuz, O., Rabkin, S.D., Martuza, R.L., Rivera, M.N., Louis, D.N., Kasif, S., Chi, A.S., Bernstein, B.E., 2013. An Aberrant Transcription FactorNetwork Essential for Wnt Signalingand Stem Cell Maintenance in Glioblastoma. CellReports 3, 1567–1579. doi:10.1016/j.celrep.2013.04.021

Sato, A., Sunayama, J., Okada, M., Watanabe, E., Seino, S., Shibuya, K., Suzuki, K., Narita, Y., Shibui, S., Kayama, T., Kitanaka, C., 2012. Glioma-Initiating Cell Elimination by Metformin Activation of FOXO3 via AMPK. Stem Cells Transl Med 1, 811–824. doi:10.5966/sctm.2012-0058

Schildge, S., Bohrer, C., Beck, K., Schachtrup, C., 2013. Isolation and Culture of Mouse Cortical Astrocytes. JoVE. doi:10.3791/50079

Seoane, J., Le, H.-V., Shen, L., Anderson, S.A., Massagué, J., 2004. Integration of Smad and forkhead pathways in the control of neuroepithelial and glioblastoma cell proliferation. Cell 117, 211–223.

Singh, S.K., Clarke, I.D., Terasaki, M., Bonn, V.E., Hawkins, C., Squire, J., Dirks, P.B., 2003. Identification of a cancer stem cell in human brain tumors 63, 5821–5828.

Suvà, M.L., Rheinbay, E., Gillespie, S.M., Patel, A.P., Wakimoto, H., Rabkin, S.D., Riggi, N., Chi, A.S., Cahill, D.P., Nahed, B.V., Curry, W.T., Martuza, R.L., Rivera, M.N., Rossetti, N., Kasif, S., Beik, S., Kadri, S., Tirosh, I., Wortman, I., Shalek, A.K., Rozenblatt-Rosen, O., Regev, A., Louis, D.N., Bernstein, B.E., 2014. Reconstructing and Reprogramming the Tumor-Propagating Potentialof Glioblastoma Stem-like Cells. Cell 1–15. doi:10.1016/j.cell.2014.02.030

Suvà, M.L., Riggi, N., Bernstein, B.E., 2013. Epigenetic reprogramming in cancer. Science 339, 1567–1570. doi:10.1126/science.1230184

Verginelli, F., Perin, A., Dali, R., Fung, K.H., Lo, R., Longatti, P., Guiot, M.-C., Del Maestro, R.F., Rossi, S., di Porzio, U., Stechishin, O., Weiss, S., Stifani, S., 2013. Transcription factors FOXG1 and Groucho/TLE promote glioblastoma growth. Nature Communications 4, 2956. doi:10.1038/ncomms3956

Vezzali, R., Weise, S.C., Hellbach, N., Machado, V., Heidrich, S., Vogel, T., 2016. The FOXG1/FOXO/SMAD network balances proliferation and differentiation of cortical progenitors and activates Kcnh3 expression in mature neurons. Oncotarget 7, 37436–37455. doi:10.18632/oncotarget.9545

Webb, A.E., Pollina, E.A., Vierbuchen, T., Urbán, N., Ucar, D., Leeman, D.S., Ben Martynoga, Sewak, M., Rando, T.A., Guillemot, F., Wernig, M., Brunet, A., 2013. FOXO3 Shares Common Targets with ASCL1 Genome-wide and Inhibits ASCL1-Dependent Neurogenesis. CellReports 4, 477–491. doi:10.1016/j.celrep.2013.06.035

Xuan, S., Baptista, C.A., Balas, G., Tao, W., Soares, V.C., Lai, E., 1995. Winged helix transcription factor BF-1 is essential for the development of the cerebral hemispheres. Neuron 14, 1141–1152. doi:10.1016/0896-6273(95)90262-7

Zhang, Y., Sloan, S.A., Clarke, L.E., Caneda, C., Plaza, C.A., Blumenthal, P.D., Vogel, H., Steinberg, G.K., Edwards, M.S.B., Li, G., Duncan, J.A., III, Cheshier, S.H., Shuer, L.M., Chang, E.F., Grant, G.A., Gephart, M.G.H., Ben A Barres, 2016. Purification and Characterization of Progenitor and Mature Human Astrocytes Reveals Transcriptional and Functional Differences with Mouse. Neuron 89, 37–53. doi:10.1016/j.neuron.2015.11.013

Zhao, S., Nichols, J., Smith, A.G., Li, M., 2004. SoxB transcription factors specify

neuroectodermal lineage choice in ES cells. Mol Cell Neurosci 27, 332–342. doi:10.1016/j.mcn.2004.08.002

Figure legends

Fig. 1 | FOXG1 and SOX2 are consistently expressed at high levels across GNS cells. A) Western blot to determine levels of FOXG1, SOX2 and OLIG2 expression across a set of GNS cells and normal NS controls. (B) ATAC-seq libraries were generated in NS and GNS cells. The 100 most differentially accessible sites across biological replicates of nine GNS cell lines and four NS cell lines were identified and are shown in a heatmap. (C) The most differentially accessible loci are enriched for key NS-specific TF motifs, most significantly the forkhead box motif.

Fig. 2 | FOXG1/SOX2 overexpression can inhibit BMP-induced astrocyte differentiation. (A) Mouse NS cell lines provide an experimentally tractable model to study astrocyte differentiation. BMP4 treatment for 24 hr is sufficient to trigger efficient differentiation: cell cycle exit, adoption of astrocyte morphological features (flattened, star-shaped), and upregulation of Gfap. (B) 24 hr after replacing EGF/FGF-2 with BMP4, morphological changes are accompanied by downregulation of Ki67 and upregulation of Gfap (C) qRT-PCR analysis shows that, at a population level, BMP4 treatment of NS cells at low density (10 cells/mm^2) results in significant downregulation of Nestin and Olig2, and upregulation of astrocyte markers Gfap, Aqp4 and S100 beta. Mean +/- SD, n=3. Significance was assessed by Student's t-test with Holm-Sidak correction for multiple comparisons (* $P \leq 0.05$, ** $P \leq 0.01$, *** $P \leq 0.001$). (D) Western blot to show Foxg1 levels in clones picked following Cre treatment of Foxg1fl/fl NS cells demonstrate biallelic excision and absent protein expression. (E) Ki67 ICC was used to score proliferation in Foxg1 ablated cells. (F) A Doxycycline-inducible transgene cassette was designed to enable inducible co-expression of FOXG1 and SOX2 (TRE, TET-responsive element; V5, V5 epitope tag;

P2A, porcine teschovirus-1 2A self-cleaving peptide sequence; PB, piggyBac; BSD, blasticidin resistance; IRES, internal ribosome entry site). Western blot (below) confirms dose-dependent increases in FOXG1 and SOX2 protein levels. (G) ICC for V5 and SOX2 confirms Dox-induced (1000 ng/ml) increase in V5-FOXG1 and SOX2 levels. (H) Clonal lines (F6, F11 and FS3) harboring the inducible cassettes (shown in Fig. 2F, S2E and S2F) were generated and transgene mRNA levels were determined by qRT-PCR following exposure to growth media supplemented with different concentrations of Dox. (I) Growth curves for mouse NS cells cultured in media supplemented with the mitogens EGF/FGF-2 (8 ng/ml each) plus BMP4 (2 ng/ml), either with or without induction of FOXG1/SOX2 overexpression by Dox (significance assessed by Student's *t*-test: FS3 +Dox vs FS3 -Dox (n=3), $p<0.001$ at all timepoints after 178 hours). (J) Phase contrast images of FS3 cells cultured in media supplemented with the mitogens EGF/FGF-2 (8 ng/ml each) plus BMP4 (2 ng/ml), with or without Dox supplementation, after 24 hr and 10 days.

Fig. 3 | FOXG1/SOX2 drives reacquisition of NS cell identity in post-mitotic astrocytes. (A) Schematic of the experimental strategy used to test de-differentiation. Cells at clonal density (10 cells/mm^2) are treated with BMP4 (10 ng/ml) for 24 hr and then switched to EGF/FGF-2 media, with or without transgene induction by Dox treatment. (B) EdU staining shows that no rapidly-cycling cells remain after 24 hr BMP4 treatment. 24 hr after plating in EGF/FGF-2 or BMP4, a 24 hr pulse of EdU was administered in media containing EGF/FGF-2. Representative images of EdU staining and quantification of % EdU positive cells are shown for each condition (Mean +/- SD, n=2 independent experiments. Scale bar: 100 μm) (C) Transgene dose determines the extent of colony formation after 10 days in EGF/FGF-2 (n=3 independent

experiments). Tumor competent IENS cells (Ink4a-Arf null; EGFRvIII overexpression) retain colony-forming ability after BMP treatment and serve as a positive control, whilst ANS4 cells serve as a negative control; below, example 10 cm dishes, for FS3 (no Dox), FS3 (Plus Dox, 1000 ng/ml) and IENS, after 24 hr BMP4 treatment and return to EGF/FGF-2 for 10 days. FS3 cells form colonies efficiently on transgene induction. (D) ICC for FS3 cells showing Gfap and Nestin protein levels after: 24 hr in EGF/FGF-2, 24 hr in BMP4, return to EGF/FGF-2 for 10 days without Dox and return to EGF/FGF-2 for 10 days with Dox. (E) Heatmap of the most differentially expressed transcripts across RNA-seq libraries at various time-points during de-differentiation; biological replicates are shown for each condition, with variability at early stages due to the low absolute numbers of cells that de-differentiate. (F) FS3 cells retain astrocytic and neuronal differentiation potential after long term expansion (~30 days), as shown by ICC for Gfap and Tuj1. (F) Mouse primary astrocytes were derived from P3 mouse cortex and the FOXG1/SOX2 inducible transgene introduced by lipofection. Following the described colony forming assay, colonies were scored two weeks following restoration of EGF/FGF-2. (G) A working model: in the presence of mitogens, FOXG1 acts to prevent and reverse differentiation commitment; SOX2 is required for proliferation.

Fig. 4 | **ChIP-seq of FOXG1 targets in mouse NS cells.** (A) FOXG1-V5 ChIP-Seq identifies 6897 binding peaks conserved across two separately derived mouse NS cell lines (Foxg1 ChIP mm10.bed). Motif analysis within the ChIP-seq peak regions for FOXG1-V5 reveals enrichment for the forkhead box motif, as well as helix-loop-helix, NF1-CTF and HMG-box motifs. (B) There is extensive overlap between FOXG1 and Sox2 bound regions with 3856 of 6897 FOXG1 bound regions also exhibiting Sox2

binding. (C) Shared bound regions were assigned to gene loci using the Stanford GREAT tool (FOXG1_Sox2 intersect gene associations.txt) and were found to be enriched for the gene ontology terms shown (FOXG1_Sox2 Intersect Gene Ontology.tsv) (D) RNA-seq demonstrates that *Foxo3* is upregulated after BMP4 treatment, along with astrocyte markers *Gfap* and *Aqp4*; by contrast, *Nestin* and epigenetic remodelling machinery *Tet3* and *Dnmt1* are downregulated. NS cell expression patterns return by day 14 (+Dox).

Fig. 5 | FOXG1/SOX2 forced expression drives reduced expression of Foxo3 and genetic ablation of *Foxo3* removes a barrier to cell cycle re-entry.

(A) RNA-seq data for Foxo3 following return to EGF/FGF-2 for 1 or 4 days, with or without Dox. FPKM = Fragments Per Kilobase of transcript per Million mapped reads. (B) ICC for FoxO3 protein in FS3 cells plated at clonal density, after: 24 hr in EGF/FGF-2, 24 hr in BMP4 and return to EGF/FGF-2 for 4 days with or without Dox (4d = 4 days). (C) The *Foxo3* locus is bound by FOXG1 and Sox2 at both the promoter region and a conserved intronic element (CIE) (indicated by red box). These regions enrich for H3K27 acetylation (top), a marker of active promoters and enhancers, and demonstrates high conservation across mammalian species (PhyloP). Clusters of the AAACA sequence comprising part of both Forkhead and Sox binding motifs are indicated by red arrows. Guide RNAs flanking the CIE were selected with a view to excision of this region by CRISPR/Cas9 (blue rectangles), along with sequencing primers for genotyping the resulting clones (yellow rectangles). (D) PCR genotyping to confirm biallelic deletion with expected single band in one line (termed FID11); FID11 retains the ability to respond to Dox and hence induce FOXG1-V5 expression, as determined by ICC (below). (E) Deletion of the FOXG1/SOX2-bound

CIE results in derepression of *Foxo3* mRNA expression in NS cell proliferation conditions (n=3, * $P < 0.02$), (F) Colony formation following Dox-induced FOXG1/SOX2 expression is abolished in CIE-deleted cells (Mean +/- SEM). (G) Western blot confirming the absence of FoxO3 protein expression in FOD3 - a clonal cell line harboring a frameshift indel mutation on the non-targeted allele. (H) Following BMP treatment, *Foxo3*$^{-/-}$ FOD3 cells divide slowly in growth conditions (doubling time ~6 days), in contrast to *Foxo3*$^{+/+}$ controls which remain cycle arrested. FOXG1/SOX2 induction, or treatment of FOD3 cells with 5-azacytidine drives rapid colony formation and proliferation to confluence (doubling time ~24 hours). (I) Colony forming assay at 10 days for de-differentiation responses in *Foxo3*$^{-/-}$ cells and those treated with 5-Azacytidine, with and without Dox. (J) ICC for Nestin and Gfap. The proportion of cells positive for nestin in representative colonies is indicated beneath the panels. See also Fig. S5D.

Fig. 6 | FOXG1 overexpression results in increased activation of regulators of DNA methylation and these may affect key polycomb target genes

(A) Colony numbers upon return to self-renewal media with or without Dox (1000 ng/ml) for 10 days, following 24 hr BMP4 treatment. Induction of FOXG1 alone in two independent lines (F6 and F11) induced colony formation at higher efficiency than in FS3. Induction of SOX2 alone (TS15) was not sufficient to drive colony formation. (B) Example colony forming assay for F6 showing colonies after 10 days in EGF/FGF-2, only on the addition of Dox. (C) RNA-seq confirms that following FOXG1 induction by Dox, BMP4-treated F6 cells re-acquire an NS cell-like transcriptional signature.

Alignment with ChIP-seq data for FOXG1 and SOX2 (left) indicates that many of the genes activated on de-differentiation are bound by FOXG1 and SOX2. (D) qRT-PCR analysis of *Dnmt1*, *Dnmt3b* and *Tet3* (Mean +/- SD, n=4. Significance assessed by two-way ANOVA with Bonferroni post-hoc test. * $P \leq 0.05$, ** $P \leq 0.01$, *** $P \leq 0.001$, **** $P \leq 0.0001$). (E) Analysis of enrichment of RRBS identified DMRs near genes marked by polycomb in mouse ES cells (ES), neural stem cells (NS) and brain. Shown are the % CpGs assayed by RRBS found near polycomb marked genes (Background, grey) compared to those in significant DMRs after either 24 hr or 10 days of differentiation (BMP increased methylation, blue and BMP decreased, orange). Significance was assessed with Fisher's exact tests (** $P < 0.01$, *** $P < 0.001$; $n = 3$). (F) Mean methylation profiles observed by RRBS in the *Foxo3* promoter including the locations of its CpG island (CGI) and Foxg1 ChIP-seq peak. Significant DMRs are shown in red together with an additional DMR that did not reach statistical significance in all replicates of the experiment (pale red).

Fig. 7 | Genetic ablation of FOXG1 in human GBM stem cells using Cas9-assisted gene targeting. (A) CRISPR/Cas-based gene targeting was used to knockout FOXG1 in G7 cells, and no protein was detectable by western blot, with a frameshift mutation demonstrated on the second FOXG1 allele in this clone (see Fig. S7). (B) Growth curve displaying percentage confluence over time for G7 and G7 *FOXG1*$^{-/-}$ cell lines, indicating that the *FOXG1*$^{-/-}$ clone proliferates at a similar rate to parental controls *in vitro.* (C) Upon xenotransplantation, wild type G7 cells expressing a GFP reporter form invasive tumours, but *FOXG1*$^{-/-}$ derivatives fail to do so (n=4 for each cell line). (D) IHC analysis of xenografts reveals the G7 FOXG1 mutant cells display: increased expression of astrocyte markers S100 beta (red) and GFAP (grey),

reduced expression of NESTIN (grey) (E), increased expression of FOXO3 (F) and decreased expression of Ki67 (red) (G). (H) Quantitation of the percentage of cells positive for GFAP, Ki67 and FOXO3, from IHC. (I) Working model of FOXG1 and SOX2 function in GBM based on this study (green cell, post-mitotic or quiescent astrocytes; brown/grey cell, radial glia-like proliferative neural stem cell). Scale bar: 10 μm; scale bar for higher magnification images in panel F: 20 μm. Students *t* test: n =4, P <0.005).

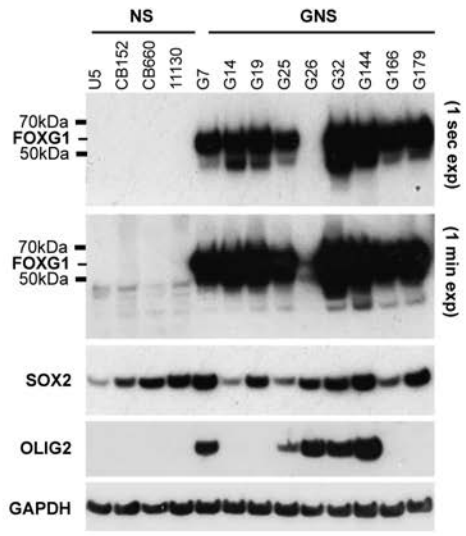

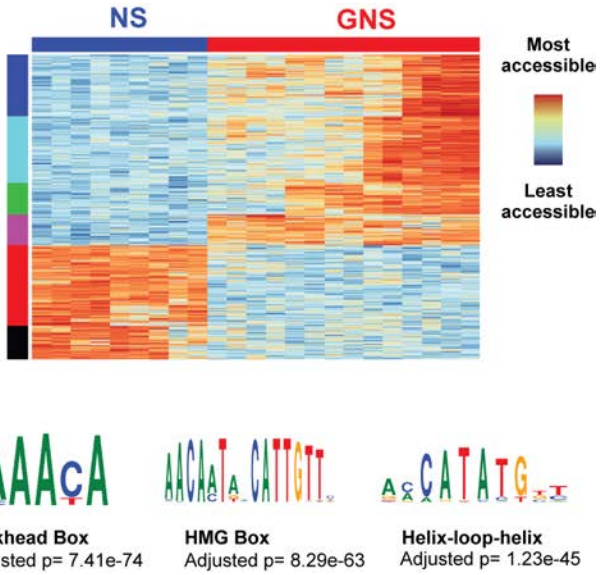

Forkhead Box
Adjusted p= 7.41e-74

HMG Box
Adjusted p= 8.29e-63

Helix-loop-helix
Adjusted p= 1.23e-45

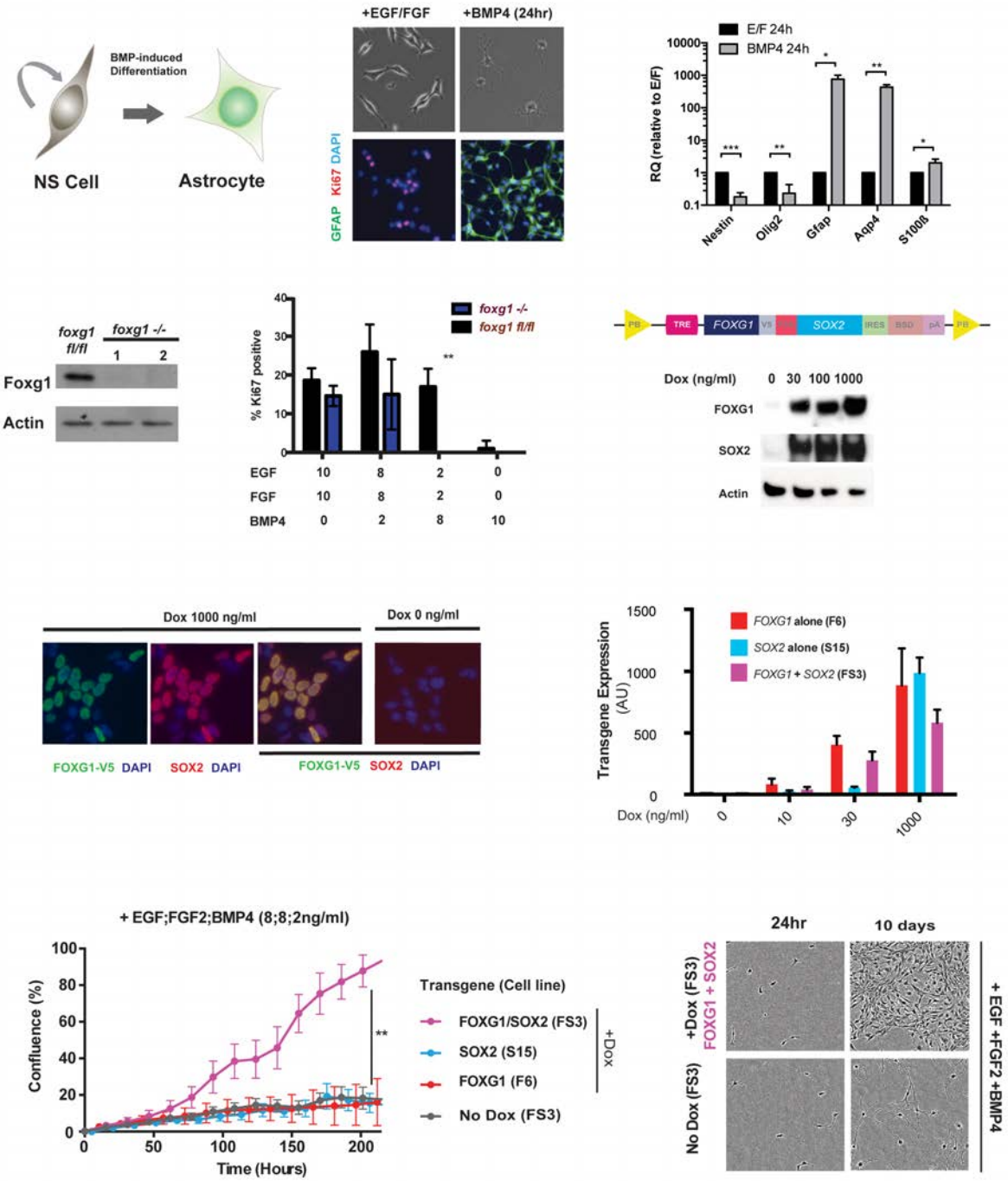
BMP-induced Differentiation
NS Cell
Astrocyte
+EGF/FGF
+BMP4 (24hr)
GFAP Ki67 DAPI
E/F 24h
BMP4 24h
RQ (relative to E/F)
Nestin
Olig2
Gfap
Aqp4
S100ß
foxg1 fl/fl
foxg1 -/-
Foxg1
Actin
% Ki67 positive
EGF 10 8 2 0
FGF 10 8 2 0
BMP4 0 2 8 10
PB TRE FOXG1 SOX2 IRES BSD pA PB
Dox (ng/ml) 0 30 100 1000
FOXG1
SOX2
Actin
Dox 1000 ng/ml
Dox 0 ng/ml
FOXG1-V5 DAPI
SOX2 DAPI
FOXG1-V5 SOX2 DAPI
Transgene Expression (AU)
FOXG1 alone (F6)
SOX2 alone (S15)
FOXG1 + SOX2 (FS3)
Dox (ng/ml) 0 10 30 1000
+ EGF;FGF2;BMP4 (8;8;2ng/ml)
Confluence (%)
Time (Hours)
Transgene (Cell line)
FOXG1/SOX2 (FS3)
SOX2 (S15)
FOXG1 (F6)
No Dox (FS3)
+Dox
24hr
10 days
+Dox (FS3) FOXG1 + SOX2
No Dox (FS3)
+ EGF +FGF2 +BMP4

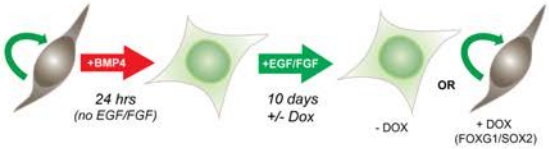
+BMP4
24 hrs
(no EGF/FGF)
+EGF/FGF
10 days
+/- Dox
- DOX
OR
+ DOX
(FOXG1/SOX2)

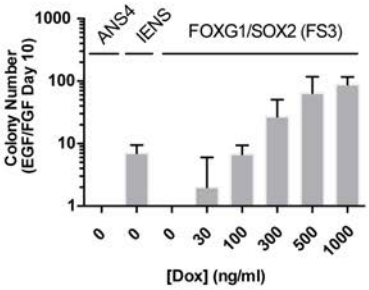
ANS4
IENS
FOXG1/SOX2 (FS3)
Colony Number
(EGF/FGF Day 10)
1000
100
10
1
0 0 0 30 100 300 500 1000
[Dox] (ng/ml)

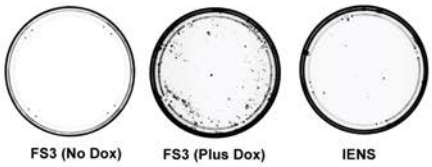
FS3 (No Dox)
FS3 (Plus Dox)
IENS

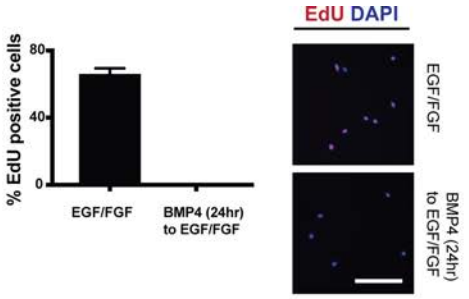
EdU DAPI
% EdU positive cells
80
40
0
EGF/FGF
BMP4 (24hr)
to EGF/FGF
EGF/FGF
BMP4 (24hr)
to EGF/FGF

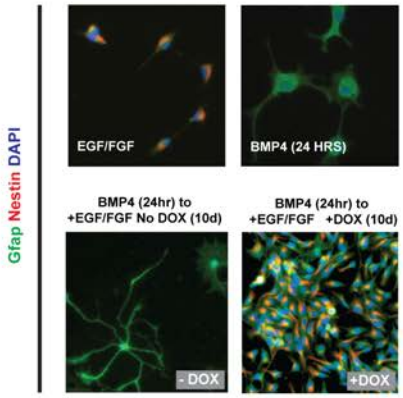
Gfap Nestin DAPI
EGF/FGF
BMP4 (24 HRS)
BMP4 (24hr) to
+EGF/FGF No DOX (10d)
BMP4 (24hr) to
+EGF/FGF +DOX (10d)
- DOX
+DOX

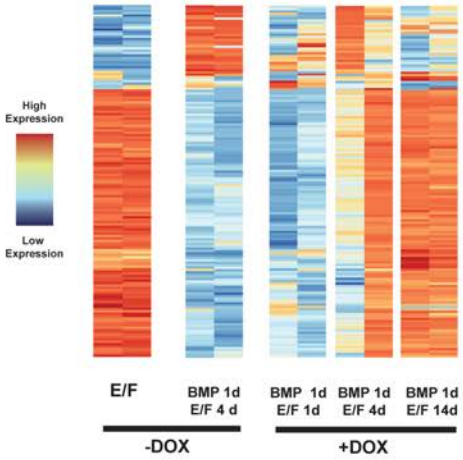
High
Expression
Low
Expression
E/F
BMP 1d
E/F 4 d
BMP 1d
E/F 1d
BMP 1d
E/F 4d
BMP 1d
E/F 14d
-DOX
+DOX

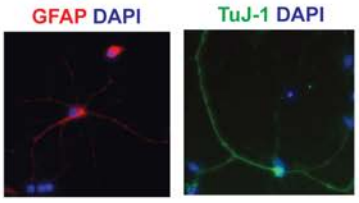
GFAP DAPI
TuJ-1 DAPI

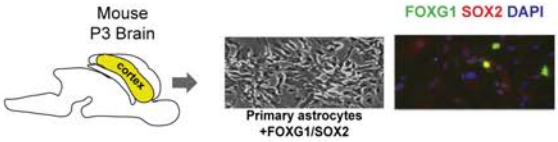
Mouse
P3 Brain
Cortex
FOXG1 SOX2 DAPI
Primary astrocytes
+FOXG1/SOX2

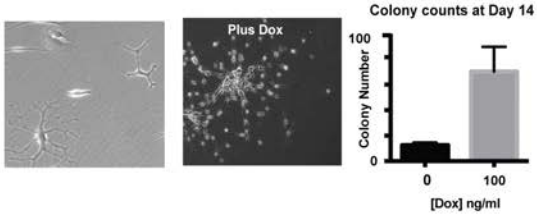
Plus Dox
Colony counts at Day 14
Colony Number
100
0
0
100
[Dox] ng/ml

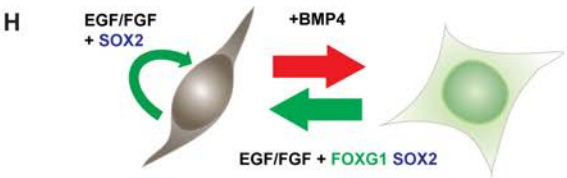
H
EGF/FGF
+ SOX2
+BMP4
EGF/FGF + FOXG1 SOX2

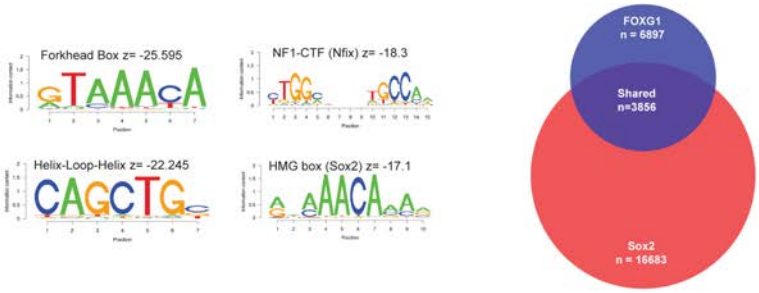
Forkhead Box z= -25.595
NF1-CTF (Nfix) z= -18.3
Helix-Loop-Helix z= -22.245
HMG box (Sox2) z= -17.1
FOXG1
n = 6897
Shared
n=3856
Sox2
n = 16683

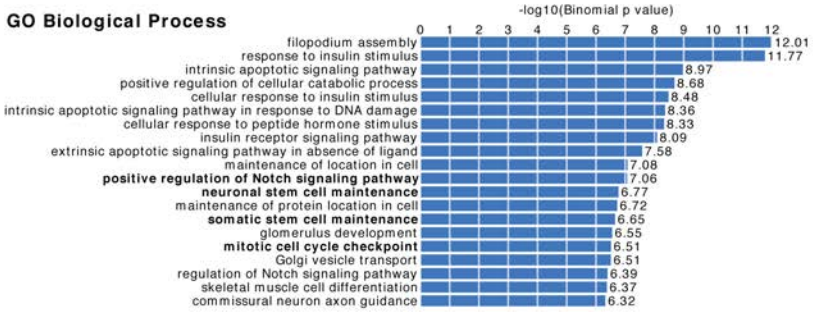
GO Biological Process
-log10(Binomial p value)
0 1 2 3 4 5 6 7 8 9 10 11 12
filopodium assembly 12.01
response to insulin stimulus 11.77
intrinsic apoptotic signaling pathway 8.97
positive regulation of cellular catabolic process 8.68
cellular response to insulin stimulus 8.48
intrinsic apoptotic signaling pathway in response to DNA damage 8.36
cellular response to peptide hormone stimulus 8.33
insulin receptor signaling pathway 8.09
extrinsic apoptotic signaling pathway in absence of ligand 7.58
maintenance of location in cell 7.08
positive regulation of Notch signaling pathway 7.06
neuronal stem cell maintenance 6.77
maintenance of protein location in cell 6.72
somatic stem cell maintenance 6.65
glomerulus development 6.55
mitotic cell cycle checkpoint 6.51
Golgi vesicle transport 6.51
regulation of Notch signaling pathway 6.39
skeletal muscle cell differentiation 6.37
commissural neuron axon guidance 6.32

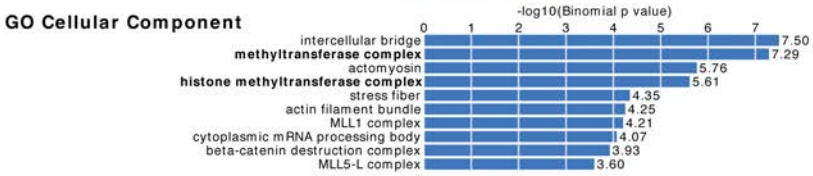
GO Cellular Component
-log10(Binomial p value)
0 1 2 3 4 5 6 7
intercellular bridge 7.50
methyltransferase complex 7.29
actomyosin 5.76
histone methyltransferase complex 5.61
stress fiber 4.35
actin filament bundle 4.25
MLL1 complex 4.21
cytoplasmic mRNA processing body 4.07
beta-catenin destruction complex 3.93
MLL5-L complex 3.60

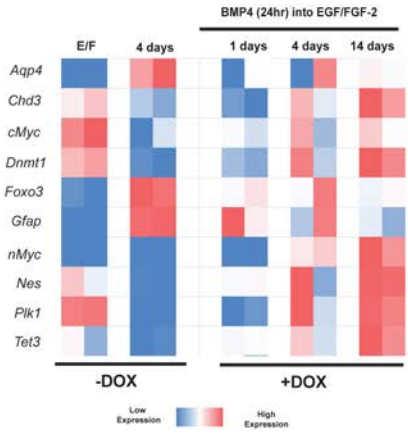
BMP4 (24hr) into EGF/FGF-2
E/F
4 days
1 days
4 days
14 days
Aqp4
Chd3
cMyc
Dnmt1
Foxo3
Gfap
nMyc
Nes
Plk1
Tet3
-DOX
+DOX
Low Expression
High Expression

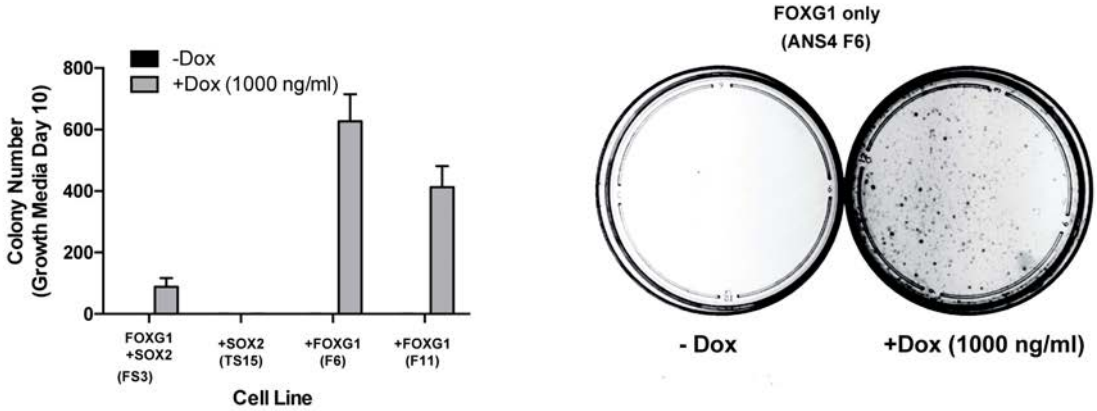
-Dox
+Dox (1000 ng/ml)
Colony Number (Growth Media Day 10)
800
600
400
200
0
FOXG1 +SOX2 (FS3)
+SOX2 (TS15)
+FOXG1 (F6)
+FOXG1 (F11)
Cell Line
FOXG1 only (ANS4 F6)
- Dox
+Dox (1000 ng/ml)

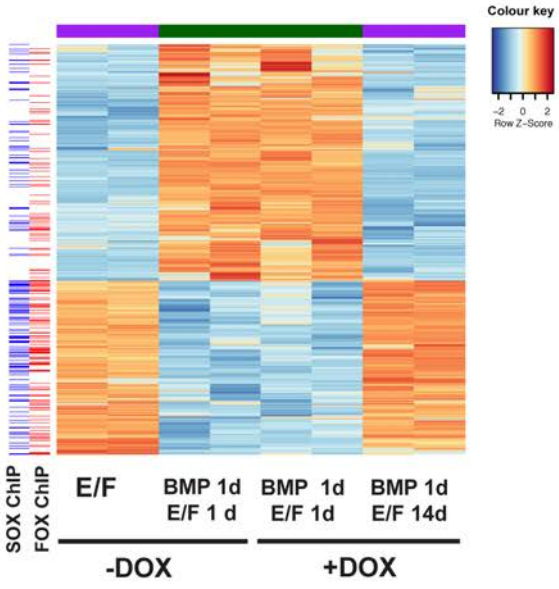
Colour key
-2 0 2
Row Z-Score
SOX ChIP
FOX ChIP
E/F
BMP 1d E/F 1 d
BMP 1d E/F 1d
BMP 1d E/F 14d
-DOX
+DOX

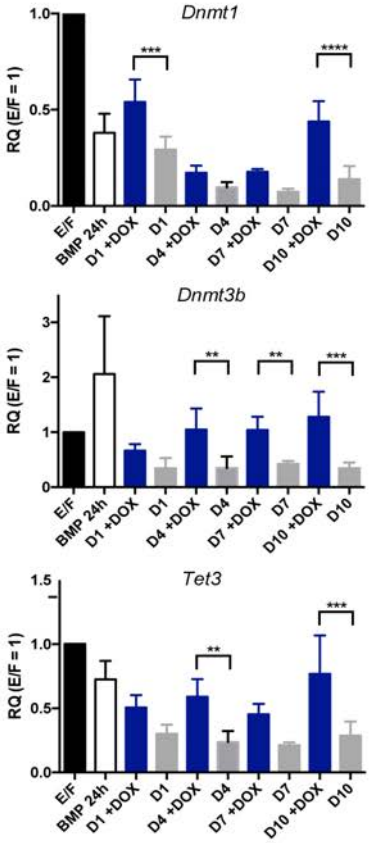
Dnmt1
Dnmt3b
Tet3
RQ (E/F = 1)
E/F
BMP 24h
D1 +DOX
D1
D4 +DOX
D4
D7 +DOX
D7
D10 +DOX
D10

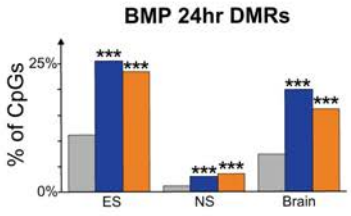
BMP 24hr DMRs
% of CpGs
25%
0%
ES
NS
Brain

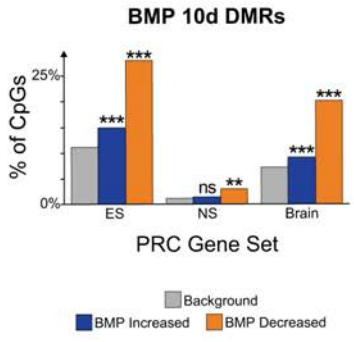
BMP 10d DMRs
% of CpGs
25%
0%
ES
NS
Brain
PRC Gene Set
Background
BMP Increased
BMP Decreased

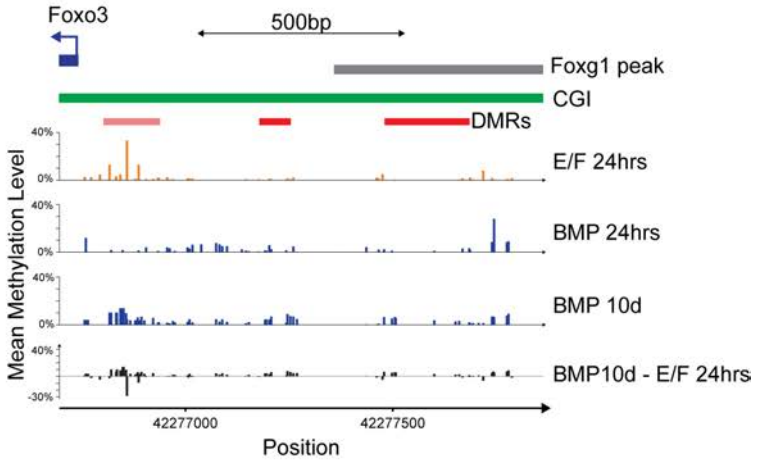
Foxo3
500bp
Foxg1 peak
CGI
DMRs
Mean Methylation Level
E/F 24hrs
BMP 24hrs
BMP 10d
BMP10d - E/F 24hrs
42277000
42277500
Position

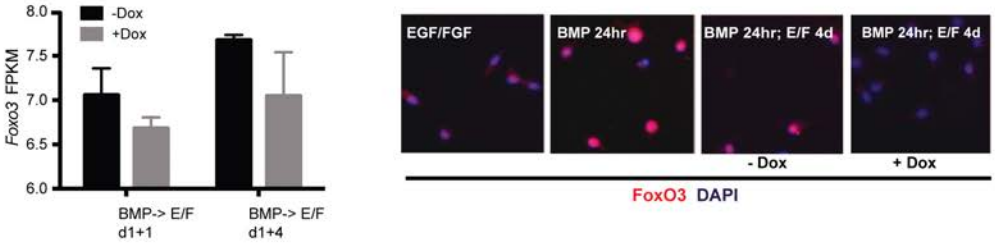
-Dox
+Dox
Foxo3 FPKM
8.0
7.5
7.0
6.5
6.0
BMP-> E/F d1+1
BMP-> E/F d1+4
EGF/FGF
BMP 24hr
BMP 24hr; E/F 4d
BMP 24hr; E/F 4d
- Dox
+ Dox
FoxO3 DAPI

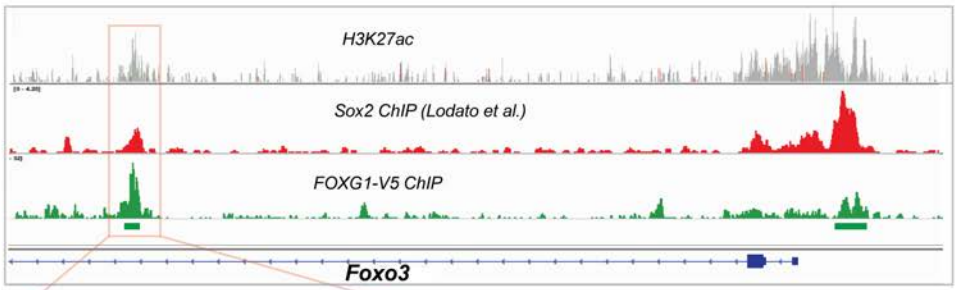
H3K27ac
Sox2 ChIP (Lodato et al.)
FOXG1-V5 ChIP
Foxo3

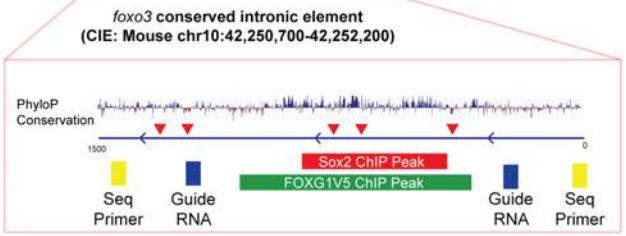
foxo3 conserved intronic element
(CIE: Mouse chr10:42,250,700-42,252,200)
PhyloP Conservation
1500
0
Sox2 ChIP Peak
FOXG1V5 ChIP Peak
Seq Primer
Guide RNA
Guide RNA
Seq Primer

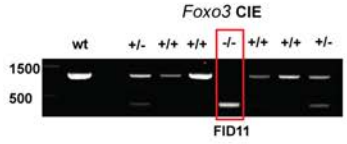
Foxo3 CIE
wt
+/-
+/+
+/+
-/-
+/+
+/+
+/-
1500
500
FID11

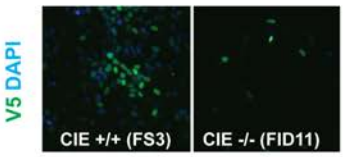
V5 DAPI
CIE +/+ (FS3)
CIE -/- (FID11)

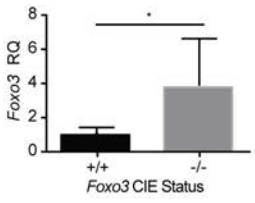
Foxo3 RQ
8
6
4
2
0
*
+/+
-/-
Foxo3 CIE Status

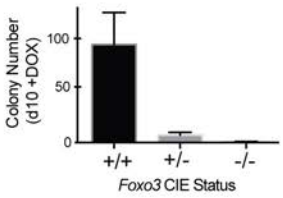
Colony Number (d10 +DOX)
100
50
0
+/+
+/-
-/-
Foxo3 CIE Status

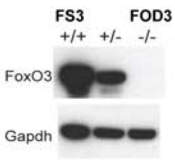
FS3
FOD3
+/+
+/-
-/-
FoxO3
Gapdh

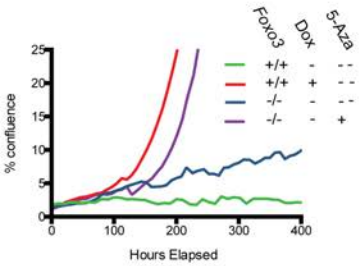
Foxo3
Dox
5-Aza
+/+ - - -
+/+ + - -
-/- - - -
-/- - +
% confluence
25
20
15
10
5
0
0
100
200
300
400
Hours Elapsed

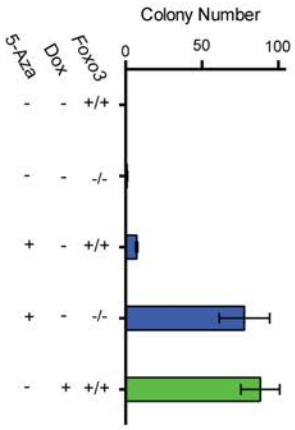
Colony Number
5-Aza
Dox
Foxo3
0
50
100
- - +/+
- - -/-
+ - +/+
+ - -/-
- + +/+

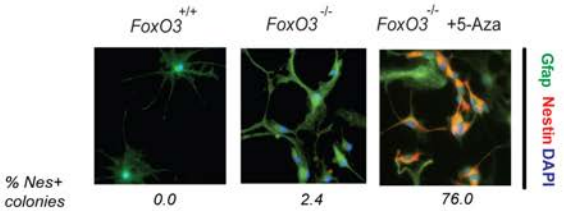
FoxO3 +/+
FoxO3 -/-
FoxO3 -/- +5-Aza
Gfap Nestin DAPI
% Nes+ colonies
0.0
2.4
76.0

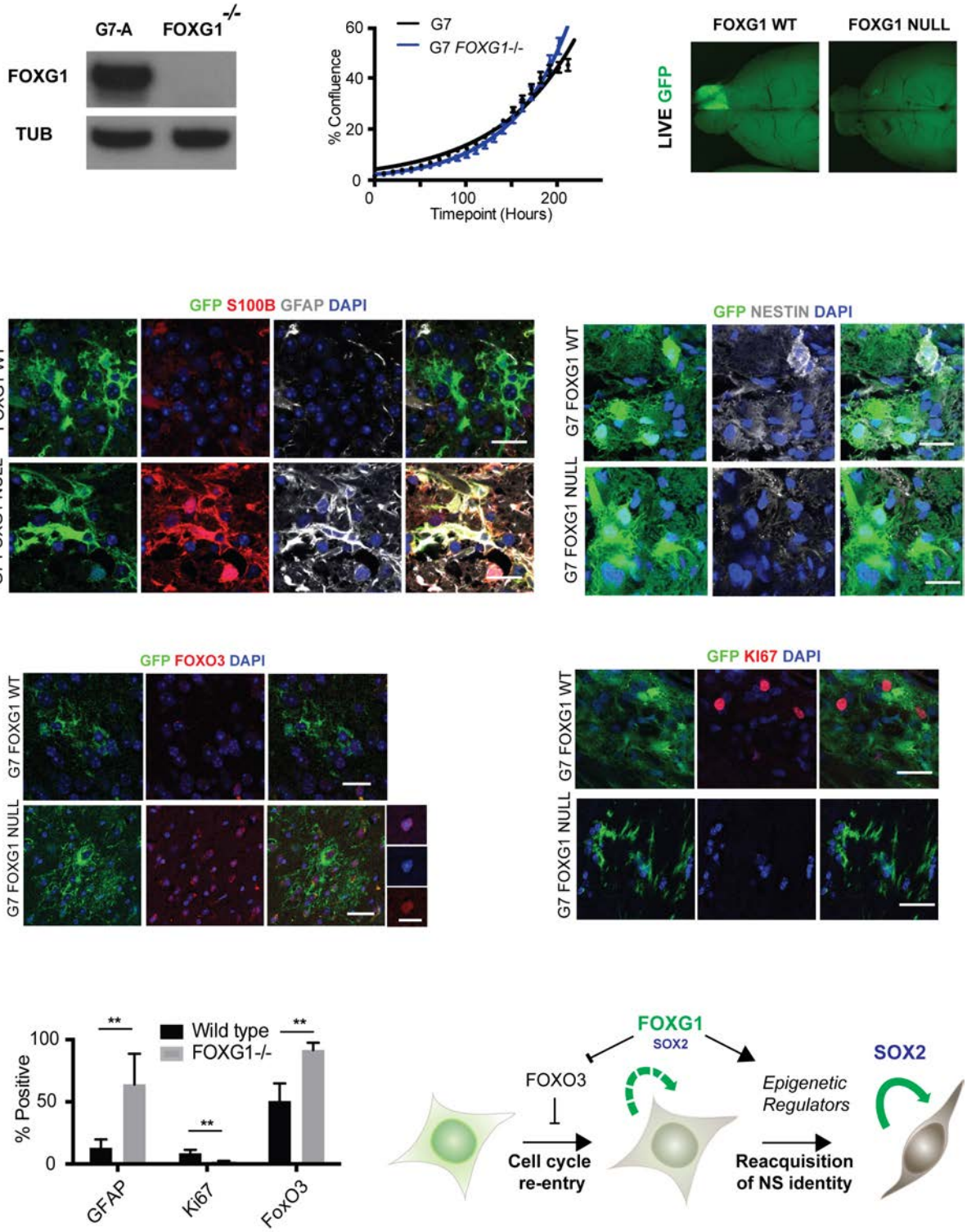
G7-A
FOXG1 -/-
FOXG1
TUB
G7
G7 FOXG1-/-
% Confluence
Timepoint (Hours)
FOXG1 WT
FOXG1 NULL
LIVE GFP
GFP S100B GFAP DAPI
FOXG1 WT
G7 FOXG1 NULL
GFP NESTIN DAPI
G7 FOXG1 WT
G7 FOXG1 NULL
GFP FOXO3 DAPI
G7 FOXG1 WT
G7 FOXG1 NULL
GFP KI67 DAPI
G7 FOXG1 WT
G7 FOXG1 NULL
Wild type
FOXG1-/-
% Positive
GFAP
Ki67
FoxO3
FOXG1
SOX2
FOXO3
Cell cycle re-entry
Epigenetic Regulators
Reacquisition of NS identity
SOX2